POLITECNICO DI TORINO

Master Degree
in Nanotechnologies for ICTs

Master Thesis

Study of atomic silicon dangling bonds for beyond-CMOS nanocomputing

Supervisor
Prof.ssa Mariagrazia Graziano
Co-supervisors
Prof. Gianluca Piccinini
Dott. Yuri Ardesi
Dott.ssa Giuliana Beretta
Relators' Sign

. . . .

Candidate
Dott. Antonio Incalza

Candidate's Sign

. . . .

Academic Year 2022-2023

A mamma, papà,
Francesca e Andrea

Summary

The need for less power-consuming and more performing devices pushed CMOS engineering up to its limits, thus new methods of performing computing and creating larger memories and faster devices are becoming a necessity as the technologies that carry this promise (More-Moore, More than Moore or Beyond CMOS). The mechanism of interaction exploited by these technologies is different from the traditional voltage-to-current relation of CMOS, carrying on collateral that cannot be addressed in a standard way because of costs or complexity.

Field-coupled nanocomputing emerges as a candidate in this landscape, with promisingly low power consumption, high-speed operation, and the intrinsic very compact size. The possible vectors used to transport information can be a variety thus a way of predicting with good accuracy and avoiding expensive ab initio simulations' computational costs has become more urgent.

This thesis exploits the adaptability of MoSQuiTo methodology, seeking to determine if it is feasible to simulate atomic components to design field-coupled circuits from atomic Silicon Dangling Bonds (SiDBs) exploiting a molecular self-consistent potential algorithm. The first phase involved the definition of the geometry, electrostatic properties, and physical behavior under an annealing schedule of SiDB-like molecules, represented by two dots interacting through a screened Coulomb potential. In this first phase, the molecule definition and post-processing phases of MoSQuiTo have been gathered together to derive the figure of merits needed for the system-level analysis. In the second stage, a self-consistent method called SCERPA (Self-Consistent Electrostatic Potential Algorithm) is employed to simulate the information transmission in the circuit after its layouts have been design. The results can then be subjected to post-processing, allowing the extraction of the most relevant physical parameters like electrostatic potential and electric field in every point within the simulation space or the charge in each molecule, thus a full acknowledgment of the propagation of the information in the circuit.

Contents

List of Figures

Part I

Introduction

Chapter 1

Context and Preambles

1.1 Alternative Computing and FCN

In the last few years, the limits of standard photolithography and CMOS technology have made more and more necessary alternative ways of designing computation and memory elements with the scope of more efficient and less time-consuming devices. Beyond CMOS, in-memory computing, More-Moore technologies for example are the candidates to obtain these results. In particular, Field Coupled Nanocomputing (FCN) has piqued the scientific community's interest in the past few years. This technology exploits different methods of information propagation concerning the standard current-based CMOS. FCN's physical mechanism of switching is based on the coupling (electrostatic, tunneling, magnetic, ferroelectric, etc....) between two entities at the nanoscale dimensions, that are capable of propagating some information, encoded in the physical properties of the cell. Due to the extreme scaling and the potential for low-power/high-frequency devices, offering key advantages such as miniaturization, parallel processing, and fault tolerance, the FCN paradigm represents an extensively studied approach for enhancing state-of-the-art computing technology. FCN finds in quantum dot cellular automata (QCA), nanomagnetic logic (NML), and silicon dangling bonds (SiDBs) its physical implementation, the binary information can be encoded either in the orientation of magnetic moments of nanomagnets (NML) or in the charge configuration of quantum dots (QCA and SiDBs) with the promise of ultra-low-power, fast and intrinsically high compact devices. Despite the distinctions in their physical characterization Quantum Dot Cellular Automata (QCA) and Silicon Quantum Dot (SiDBs) share highly similar abstract models. This allows algorithmic principles to be available for both technologies within the nanocomputing domain.

Unlike conventional silicon-based technologies, QCA employs quantum dots (QDs) cells typically composed of 4/6 of these semiconductor nanostructures which are usually identified with particular molecules (i.e.: Bisferrocene, butane, decatriene etch) [8][3], usually 4 to encode the information and 2 for the reset/null state. In QCA, electrons are free to tunnel within QDs in the cells but aren't between cells, their mutual Coulombic interactions are exploited to obtain determined charge configurations to execute logic operations. However, bringing higher device density and faster switching mechanisms creates the problem of modeling and implementing complex interacting systems. The Coulombic nature of the interaction allows to discard of the traditional current-to-voltage interaction of classic silicon-based technology thus allowing for faster and less power-consuming devices. FCN circuits are assumed to evolve adiabatically with the cells tracking the ground state of the neighbors, except for errors due for example to thermal excitation or wrong geometrical characterization. In general, to obtain a correct representation of the interactions a quantum mechanical approach should be taken into account anyway considering only electrostatic interactions can be an acceptable approximation. [5][4]

When a cell is in proximity to and interacts with an electrode, it takes one of its two polarized states, delineating the logical '1' or '0'. The adjacent element then mimics this configuration to transmit the input state to the opposite side of the circuits.[1] The electron transfer (switching) can be spontaneous leading to errors or controlled, for example, it can be triggered with an electrical signal that controls inter-dot electron occupation called a clocking signal, or some other parameter (for example carrier population in SiDBs). Typically the cells are placed in a grid and the distance and reciprocal orientation dictate the strength of the inter-cell coupling. Organizing the circuit in blocks having different clocking signals called pipeline organization makes it possible to safely switch cells' subarrays in which the circuit has been divided, limiting the uncertainty of propagation due to long distances. [9]

1.2 Quantum dot Cellular Automata

In QCA, information is encoded into cells made of quantum dots. As shown in 1.1, the cells typically consist of four quantum dots placed at the corners of a square and two smaller dots exploited to be able to impose a reset/null phase over the cell. Different cell arrangements result in different interactions between the electronic configurations of each cell. In general, the Coulombic repulsion causes the electrons to occupy opposite corners of the cell, forcing the arrangement into one of two antipodal (or "diagonal") configurations or else the lower energy configuration available to the system. Between the cells no charge transfer occurs, the electrons change their position among cells due to Coulombic repulsion while inside a cell they can freely tunnel depending on the external condition like the electric field imposed over the circuit.

A clock zone is a group of cells whose parameters can be set to make a group of cells polarized or non-polarized (activate or deactivate a cell within a specific clock zone). A bit of information can sequentially travel across the circuit, consisting of a group of cells interacting in "active" clock zones exploiting the pipeline concept of utilizing different phases to activate different pieces of the circuit at different time moments to speed up the propagation and obtain a more trustful signal. A single QCA circuit can process many bit packets simultaneously by modulating the clock zones accordingly.[9][7][10] Therefore, a simple row of cells can act as a binary wire and can propagate information like the example in 1.2

Despite the QCA cells are difficult to model due to quantum effects large groups of cells can be addressed by applying different approximations that allow simplifying the otherwise fully quantum mechanical problem that for a cell containing i,j dots reads:

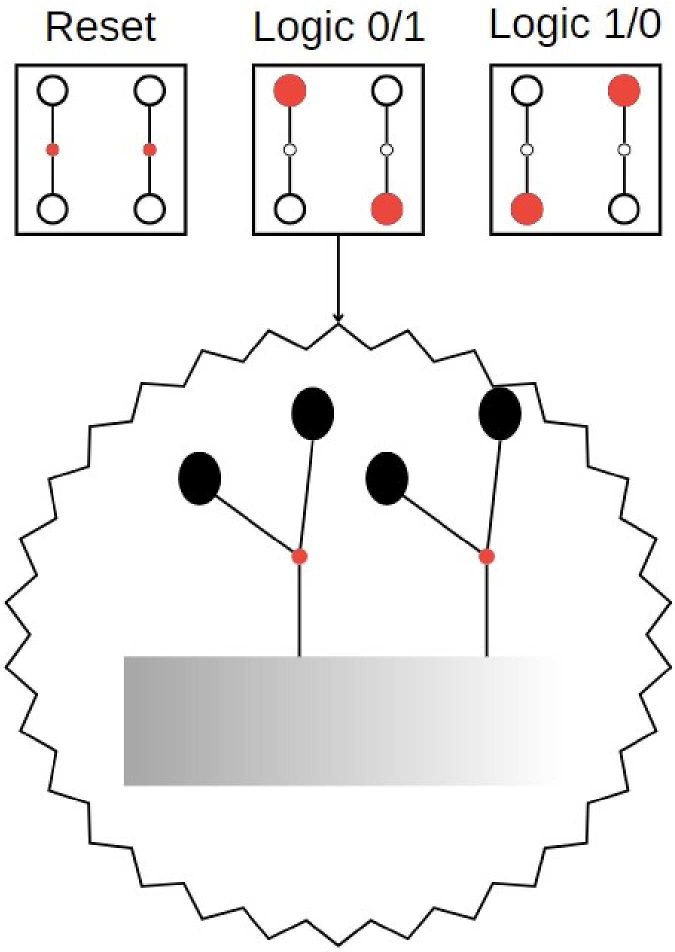

Figure 1.1: Example of typical 6 dot cell for QCA framework, the bigger molecules are used to retain the charge during the computing and thus are the actual computing elements while the smaller dots are used to be able to impose a reset phase.

$$H^{\hat{cell}} = \sum_{i,\sigma} (E_0 + V_i)\hat{n}_{i,\sigma} + \sum_{i>j,\sigma} t_{i,j}\hat{a}^{\dagger}_{i,\sigma}\hat{a}_{j,\sigma'}\hat{a}^{\dagger}_{j,\sigma'}\hat{a}_{i,\sigma} + \sum_{i} E_Q \hat{n}_{i,\uparrow}\hat{n}_{j,\downarrow} + \sum_{i,j,\sigma,\sigma'} V_Q \frac{\hat{n}_{i,\sigma}\hat{n}_{j,\sigma'}}{|\mathbf{R_i} - \mathbf{R_j}|} \tag{1.1}$$

where $\hat{a}_{i,s}$ ($\hat{a}^{\dagger}_{i,s}$) represents the annihilation (creation) operator for an electron on-site i with spin σ. $\hat{n}_{i,s} = \hat{a}^{\dagger}_{i,s}\hat{a}_{i,s}$ is the number operator. The first term is the on-site energy of each quantum dot. The electron potential energy V_i accounts for charges outside the cell. The second term captures electron tunneling between adjacent sites, with $t_{i,j}$ hopping constant for neighboring sites. The third term represents the energy costs E_Q of placing on the same site two electrons having opposite spin. The last term corresponds to the Coulombic interaction among electrons placed on distinct sites within a cell. [7][11]

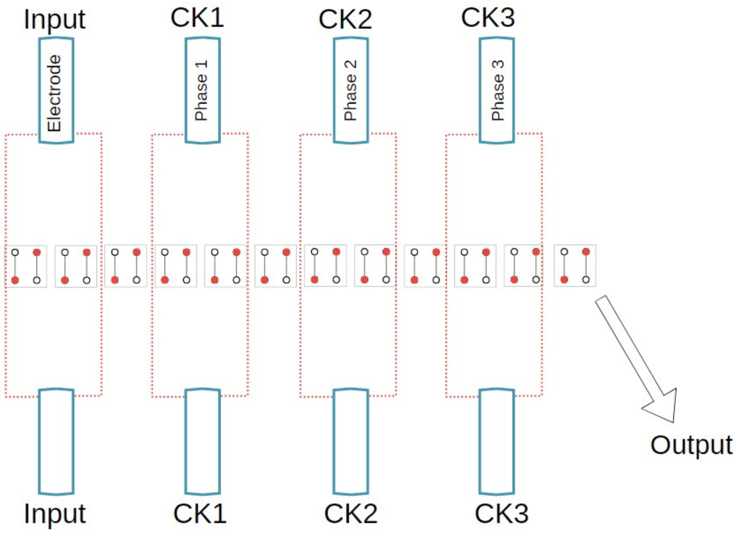

Figure 1.2: Example of pipeline organized QCA wire, the clocks are implemented to be able to activate different circuit's zones in different moments thus favoring information propagation and stability along more complicated circuits.

This problem has been assessed with different approximations allowing not only simpler modeling of the cells but also the possibility of simulating more complex QCA circuits. Some of these approximations includes: [9][7][10][11]

- A mean-field approach to the inter-cell interactions involving approximating the interaction between cells by considering the average effect of neighbors;
- The reduction of the otherwise sixteen-dimensional Hilbert space, solution of the two-cell's polarization Hamiltonian (1.2) to a two states solution representing the diagonal and anti-diagonal states:

$$H = -\sum_{i=1}^{N} \gamma_i \hat{\sigma}_x(i) - \frac{1}{2}\sum_{i<j} E_k^{i,j} \hat{\sigma}_z(i)\hat{\sigma}_z(j) + \frac{1}{2}\sum_{D}\sum_{i=1}^{N} E_k^{i,D} P_D \hat{\sigma}_z(i) \tag{1.2}$$

  with γ_i effective tunneling energy, $t_{i,j}$ hopping constant, $E_k^{i,j}$ kink energy that accounts for the energetic cost of two cells with opposite polarization, with the D labeled the driver's term having polarization P_D which acts as input for the system. Let's denote the quantum states of a single quantum dot as $|0\rangle$ and $|1\rangle$, corresponding to the absence and presence of an electron, respectively. The quantum state of the entire QCA system can then be expressed as a product of these states for each quantum dot;
- The cell-cell interactions include the assumption of exponential energy relaxation referring to the exponential decay of the probability amplitude for a quantum system to be in a certain state over time:

$$P(t) = P(0) \cdot e^{\frac{-t}{\tau}} \tag{1.3}$$

with P(t) probability of the system being in a certain state at time t, P(0) is the initial probability, and τ the relaxation constant of the system;

- The adiabatic approximation refers to a situation where a system evolves slowly compared to the characteristic timescale of changes in its Hamiltonian;
- The relaxation time approximation for which in the absence of decohering effects the QCA ensembles are assumed to evolve coherently and thus can be described by a Liouville equation which can be integrated at low-temperatures with a dissipative term, under the conditions that cells are weakly coupled and the system can be described with a Markov process (random process indexed by time with the property that the future is independent of the past)[7]:

$$\frac{d}{dt}\hat{\rho}(t) = \frac{1}{i\hbar}[\hat{H}(t), \hat{\rho}(t)] - \frac{1}{\tau}(\hat{\rho}(t) - \hat{\rho_{ss}}) \tag{1.4}$$

with τ an empirical time constant and $\hat{\rho}_{ss}$ steady-state matrix.

These approximations have significantly advanced the field of simulating devices from small cell groups to large QCA gates.[7][10][11] This work seeks to avoid the solution of difficult quantum mechanical systems for an alternative framework to FCN such as silicon dangling bonds (SiDB) taking advantage of a more engineering approach that allows to asses of the atomic environment of this technology exploiting only an electrostatic approximation of the basic SiDB cell composed of a couple of dots which can resemble the basic component of a QCA cell.

1.3 QCA Limitations

By now all the basic circuit elements have been modeled and experimentally demonstrated but more complex architectures have yet to be realized. Until the recent works, all available QD structures typically consisted of thousands of atoms with narrowly spaced energy levels requiring ultra-low temperatures to exhibit the electronic properties needed for the information transfer. Moreover, to control electron occupation a large number of connections were required, greatly limiting the circuitry complexity. A prospect for highly complex and room-temperature operational QCA circuitry suddenly emerged with the discovery of atomic silicon quantum dots.[1]

Recently the silicon technology progress allowed for visualization and influence of chemical reactions at the atomic scale, representing a good promise in reducing QCA limitations: inducing artificially the hydrogen desorption from the H-Si(100)2x1 surface it is possible to edit DBs and producing low power atomic circuits.[5] With atomic silicon quantum dots technology, the potential of creating intricated circuits operating at non-cryogenic temperatures is within reach.[12],[1]

During the last few years, thanks to the advancements in Scanning Tunneling Microscopy (STM) and Atomic Force Microscopy (AFM) technology, atomic manipulation has been made possible, thus the possibility to engineer specific surfaces and to build atomic circuits with desired physical properties.[5] In particular atomic manipulations of the H-passivated Si(100)2x1 surface led to the implementation of the Silicon Dangling Bond technology in an automated way, which led to the experimental demonstration of some computing building blocks like logic gates and wires.[12][13]

1.4 Silicon Dangling Bonds (SiDBs)

A silicon dangling bond (SiDB) is a desorbed hydrogen atom on the hydrogen-passivated Silicon(100)2x1 surface (H-Si(100)-2x1). It is approximately an sp^3 orbital that results in a positive, neutral, and negative charged dot when it is occupied respectively by 0, 1, and 2 electrons. [5] The information in this kind of QCA is encoded in the position of the charge between a pair of adjacent DBs that becomes like a basic molecule in standard FCN technology, thus one of the aims of this thesis will be to characterize electrostatically and physically such a couple, to make it analyzable with already tested tools like the self-consistent electrostatic potential algorithm (SCERPA) developed by the VLSI laboratory at the Politecnico di Torino [14].

This technology allowed a sub-30nm^2 OR gate and wire with the promise of a low power and high frequency operation leading the FCN implementation to a new dimension of scaling, even more compact than molecular implementation. Due to the atomic sizes of the elementary component, the DB framework is a promising candidate for building complex, low-power, and ambient-temperature working circuits.[5]

The very small size of the atomic Silicon Quantum Dots (ASiQDs) has as a consequence a very wide spacing between energy levels, allowing for good behavior at room temperature. SiDB gates operate by managing electron populations and promoting favorable electronic configurations based on varying input conditions. These conditions can be manipulated during computing for example via a clocking signal or may be linked to material or surface properties, these two approaches have different flexibility because changing the material's properties while the circuit is working results to be an inconvenient operation.[13] A sufficiently close placement of dots leads the neighbors to interact and due to Coulombic repulsion, the extraction of an electron to the silicon substrate conduction band from the pair occurs, this effect is called "Self-biasing" and allows for a precise control of the SiDB's electron population via Fermi level alteration.[1] Atomic dots are identical thus their placement occurs in an exact registry according to the atomic structure of the underlying Si crystal lattice, this allows for a high degree of homogeneity while characterizing physical properties.[1]

The materials stability of the system up to T >200 °C is comparable to conventional electronics, furthermore, fabricated DBs are expected to migrate due to thermal activation only once every 500 years at room temperature. [12] At a frequency of 1 GHz and a temperature of 77 K (liquid nitrogen), the power dissipation of the clock schemes was found to be approximately 10-100 µW cm^{-2}. At 1 THz, these power densities rise to 1-10 $\mu W cm^{-2}$. The inherent silicon nature of this technology indicates a natural compatibility with CMOS technology.[13] This thesis aimed to understand the behavior of SiDB circuits using SCERPA (Self-Consistent Electrostatic Potential Algorithm) an algorithm capable

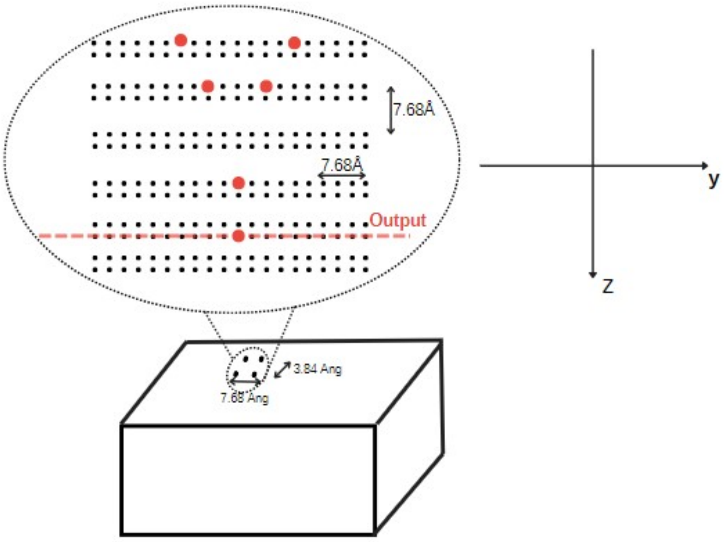

Figure 1.3: Si-H surface example, each dot represents a Si-H bond where a DB can be functionalized, the red dots are placed as an example of the OR gate firstly presented in [1]

of predicting the behavior of complex FCN molecular circuits exploiting electrostatic relations. To be able to predict the behavior of complex atomic ensembles exploiting a molecular simulator the set-up of the modeling has been based on the previous work in [5] and [6] thus breaking down to the simplest case the interaction of SiDBs to obtain a reference behavior for the simulator to run multiple interactions. To achieve such a goal an eased approach to Mosquito methodology was exploited, thus looking for a simplified description of a basic SiDB molecule adaptable to simulate circuits with good agreement with previous findings. The simplest molecule made of two atomic SiDBs has then been electrostatically characterized via the occupation of the single components, this characterization was useful to feed SCERPA with the basic information about the electrostatic of the system which was used to obtain the charge configuration of more complex circuits consequently the application of an input voltage and clocking signal. The simulations could be used as an affordable benchmark to understand the behavior not only of molecular circuits but also of atomic circuits, remarking the flexibility of the self-consistent approach, that can be adapted to smaller components like atomic silicon quantum dots. Virtually the approach used in this thesis could be adapted to any FCN building block with a basic definition of the electrostatic of the minimum component, in the particular case of the SiDBs the occupation of a couple was implemented to simulate a wire and a Y-shaped OR gate, moreover after some case characterization it was found that the Fermi statistic of a decoupled symmetric system was enough to let SCERPA define the interaction between molecules. In other words, it was not needed to define the interaction between the atoms of the couple used as a building block to feed to the algorithm the correct figure of merit used to calculate the circuit's charge configuration, the self-consistency of the algorithm was enough to predict the behavior of interacting couples even if defined with only with a symmetric, non-interacting Fermi statistics thus opening to the simulation of virtually any kind of FCN elements via self-consistent electrostatic equations.

Chapter 2

Fabrication Processes

2.1 Hydrogen Lithography

Silicon DBs are fabricated by desorption of individual hydrogen atoms from a hydrogen-terminated silicon surface using the probe of an STM. The H-Si bond is broken by applying a voltage pulse at the H site and leaves a valence orbital on the interested site. The hydrogen atoms are placed on top of the Si(100) surface with a H-to-Si ratio of 2x1, the locations of H atoms are thus discretely defined by the lattice structure periodicity of the silicon surface, allowing for a repeatable creation of SiDBs at atomically precise spots. [15] To create a single DB the tip of an STM is placed at a distance of around 4Åon top of an H atom, the feedback loop of the STM is switched off and a voltage pulse of around 2V is applied for a few milliseconds. This process resulted in an H atom transferred to the tip apex the 50% of the time while in the 30% of the cases, it was still on the surface in a site near the DB, in the last 20% of cases the H has been probably absorbed by the tip or ejected.[5] The resulting DB appears as a bright protrusion surrounded by a dark halo (a strong contrast enhancement) that can be seen from the STM images of the surface.

Moreover, it is possible to vertically manipulate a single H atom with the tip of an AFM also allowing a characterization of the chemical reactivity of the DB. The AFM allows probing the electronic properties (i.e.: charge configuration and functionality of the circuit) with minimized tip-induced band bending and e^-/h^+ injection. A single hydrogen atom can be deposited on the surface by bringing the apex of the H-functionalized tip of the AFM very close to a DB site, this allows for the mechanical creation of a covalent bond between the DB and the H atom at the tip apex which result to be re-adsorbed on the surface. Thus the AFM allows for a chemical reactivity tuning with the precise mechanically induced desorption of the H atom from a functionalized tip to the surface. Different from STM, the AFM enables a non-destructive editing of the DB structures. [5] To check the correct action of the tip on the surface it is necessary to control the frequency shifts concerning the displacement curves ($\delta f(z)$) of the AFM measures.

The AFM approach faces limitations in achieving fast, large, and error-free circuit fabrication. This happens because the frequency shift signal used in AFMs necessitates two independent feedback loops, constraining the overall process's speed. Moreover, the process may experience further delays due to the requirement of re-functionalizing the tip with hydrogen in between each event. To build large error-free atomic structures new techniques capable of a precise control of the desorption of hydrogen atoms were needed, hence a technique capable of treating multiple sites in short periods. [12]

2.2 Automated Hydrogen Lithography and Hydrogen Repassivation

Hydrogen Lithography (HL) is the technique allowing the depassivation of H atoms from the H-Si(100) 2x1 surface, leading to the creation of the DBs without introducing processes that can result incompatible with the semiconductor's state-of-the-art technology. Hydrogen Repassivation (HR) is the opposite process, consisting of repassivating a DB to erase it and correct errors. The limitations of HL were found to be in the creation of large error-free circuits thus an automated method for desorbing/adsorbing H atoms from the surface was essential. [12]

The precise position of each H atom must be known to automate HL and to have a precise STM tip pattern during the fabrication process since even a nanoscale dimension mismatch might result in the removal of the incorrect atom. The periodicity of the 2x1 H-Si(100) surface allows the location of every H atom on the surface from a single STM image through the Fourier analysis. Once the surface has been characterized, the tip is brought close to the site that must be edited and a 20ms voltage pulses of 1.8-3V and 50pA are applied at fixed tip height until the H removal is detected. Using this procedure the probability of uncontrolled degradation of the tip apex is low and more than 10 DBs can be created consecutively without changing the tip. HL process is not so sensitive to tip apex changes although an automated tip-forming routine could be used to reshape it using controlled crashes on the surface when needed. [12]

To correct errors occurrence the STM tip has been used to address individual lattice sites with atomic precision in a process called automated HR. Both Si and metal tips were found to be capable of repassivating a DB site. After the functionalization of the tip with an H atom, it is positioned over the DB with a voltage of 1.4 V and a current of 50 pA. The feedback control is turned off and the sample voltage is taken to 100 mV ÷ 1 V. While recording the tunneling current the tip is brought to 500-800 pm towards the sample and then retracted to its original position, the voltage is taken to 1.4 V and the feedback loop is turned on again. Once automated this entire process lasts 1s.[12] It is also possible to repassivate DBs using a non-functionalized tip. Furthermore, STM tips are capable of adsorbing on its surface during HL multiple H atoms,[5] a consequence of this is the chance to repassivate from 3 to 5 DBs without the need to successively load the tip.[12]

To check the correct passivation of the DB site two different types of signatures have been identified as indicators: Type-I signature: a tunneling current fast increment recorded approaching a surface with a successfully passivated DB. This signature relies on a particular tip state to enable H transfer. Type-II signature: a reduction in the tip-orbital overlap due to a reduction of the passivated DB surface orbital can lead to sudden decreases in tunneling current. Concerning the type I signature that relies on a specific orbital of the tip type II has fewer boundaries.[12]

The problems inherent to scanning probe lithography at non-cryogenic temperatures, which can bring uncertainty in the tip position leading to wrong sites (re-)passivation called creep, and thermal drift have been addressed by implementing a periodic image realignment into the workflow. Before initiating the HL process an area of $10x10nm^2$ is imaged as a reference, after a set time lithography is paused and the same area is re-imaged to see how much the tip has been displaced from its intended position. By reducing the interval between different checks the realignment efficacy can be increased.[12]

Chapter 3

Physical Properties

3.1 General Characterization of SiDB

A SiDB can be built by desorption as mentioned in the previous chapter, resulting in an sp^3 orbital, which is capable of containing a maximum of 2 e^- corresponding to the negative charge state (DB-), while a single electron occupation related to the neutral state (DB0) while to zero electrons corresponded the positive charge state (DB+). The periodicity of the H-Si surface allowed defining a constant pattern for the possible positions of the DBs which from the Si lattice constants resulted in:

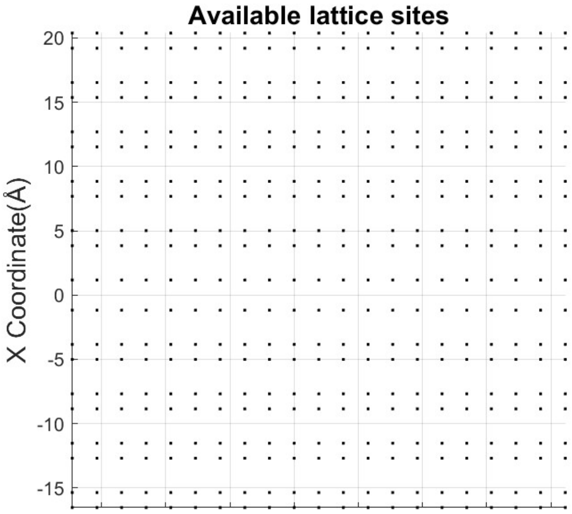

Figure 3.1: Si-H surface schematics of the available lattice sites hosting an H atom that can be functionalized to create an atomic SiDB, each dot represents a Si-H bond.

In a silicon crystal, the atoms create bands by bonding and anti-bonding with neighboring and distant silicon atoms, as a result, the zero-dimensional electrical properties are lost. Si atoms with one dangling bond and three regular Si-Si bonds have a unique mixed nature. Similar to silicon atoms with four bounded coordinates, these atoms are tightly tied to the lattice and play a crucial part in the dispersive bands that delocalize electrons. Atoms presenting three bounded coordinates (a SiDB) have one localized state, which is roughly similar to an sp^3 orbital. Since it is placed in the center of the band gap far away from the valence and conduction band, this state can be considered localized.

It has been shown that an H-Si surface having a relatively high n-type doping lets the DBs functionalized on it behave like a deep n-type dopant, ultimately allowing it to assume a negative charge configuration resulting in a dark halo protrusion from STM images, while in the case of moderate n-type doping a neutral state have been identified which correspond to a white protrusion in the STM images. The localization of the negative charge in the DB- caused a destabilization of the electron energy level called upward band bending, thus the DB can be seen as a dopant with a deep acceptor level because compensates the n-type doping effect by shifting up the energy bands with respect the Fermi level. The instantaneous charge state of a DB is influenced by the kind and concentration of the dopant, the concentration of DBs on the surface, the local electric field, and the amount of current flowing through the DB. [1]

The DB has ionization or affinity energies that are one order of magnitude higher than those of common dopant atoms, moreover, the DB state's spatial extension within the solid reaches several bond lengths, which is significantly smaller than the size of a typical dopant atom highlighting again the zero-dimensional character of SiDBs, combined with the capacity to exhibit three charge states leads us to identify the SiDB as a quantum dot. Charges on SiDBs tend to occupy the lowest energy configuration, typically involving maximizing the distance between charged elements, exploiting this behavior it is possible to fabricate logic gates by adjusting the SiDB pattern on the surface. [16]

3.2 DB to Conduction Band Tunneling

The energy levels for the first and second electrons to be found in the DB orbital are called transition levels, respectively +/0 and 0/-. The energy levels are associated with the transitions between charge states, although there exist three charge states the transition levels will result to be only two as will consequently be the energy levels involved in the charge dynamics. Moreover, it would be fallacious to assign a third energy level to the DB+ state because the absence of electrons does not allow for to definition of an "electronic energy level". Consider now the positive charge state as related to the energy of the second hole of the DB. To analyze this a hypothetical experiment firstly carried on in [7] can be exploited: Consider the symmetry between electrons and holes, and imagine a discrete unoccupied energy level near the surface called trial level (TL), it would be possible for it to experiment tunneling (gaining or loosing electrons) when crosses the DB+/- levels, a resonance condition is then said to be met. Imagine now moving the trial level across the band gap from the top to the bottom, the first resonance condition is the one with the DB- level, since this trial level is empty an electron can freely tunnel from the DB to the TL. Further lowering TL the resonance with DB0 is met, again the TL is unoccupied and the e^- lying in DB0 can be transferred. If TL meets the DB+ state nothing occurs because both states are empty. Considering again a TL but this time filled and connected to the reservoir, rising TL from the bottom of the band gap if a symmetric situation is met the hole should be transferred from the DB to the TL but this cannot occur since the minimum energy to obtain an electron transfer (thus a hole transfer) is the one corresponding to one electron in the DB corresponding to the DB0 charge state. Finally, we can conclude that the DB+ charge state can be neglected in the DB dynamics because it cannot influence electron or hole configurations. [7]

Summarizing SiDBs can be seen as atomic quantum dots with three possible charge states, previously defined as DB0, DB+/-. The transition levels between different charge states are located inside the silicon band gap and the electron occupation of the DBs is determined by the position of these transition levels with respect to the Fermi level. The transition levels can be shifted by applying an external bias thus allowing the electron population control of the SiDBs. As the bands bend upwards or downwards by external bias at the silicon surface, the transition levels shift by the same amount, as a result when the transition level crosses the Fermi energy level the SiDB experiences a change in electron population/occupation. [16] [6]

3.3 SiDB Ensembles

A closely positioned pair of dangling bonds (DBs) undergoes a significant Coulombic repulsive interaction, causing one electron to separate from the pair. This reduced net charge stabilizes the remaining electron while generating an unoccupied energy level on one of the DBs. Because the energy barrier separating the DBs is low, of the order of several 100 meV, and also very narrow (of the order 2 nm), tunneling events to the vacant state are very probable. So fabricating a pair of DBs with a similar spacing may be referred to as tunnel coupled. In [1] the best distance between DBs to obtain the optimal tunneling rate was found to be 3.84ÅDBs corresponding to an extremely short tunneling period of the order of 10 femtoseconds making this the periodicity of the crystal structure the tunneling will be favored. Conventional larger and widely spaced dots would have a tunneling rate orders of magnitude lower.

If the separation between DBs is sufficiently large the Coulombic interaction results weaker and adding the screening of conduction band electrons both the DBs of the couple assume a negative charge configuration. Otherwise closely placed dots resulted to demonstrate a “Self-Biasing” effect (SBE): the stronger Coulombic repulsion permits the extraction of an electron from the pair to the silicon substrate conduction band, due to this effect the couple of closely placed DBs can host only one extra e^-, making possible to obtain precise control of electron population altering the Fermi level. Fabricating dots with appropriate spacing is possible to pre-determine the e^- configuration eliminating the wiring problem of FCN.[13]

In symmetric square or rectangular cells, the freely tunneling electrons can occupy with the same probability the degenerate diagonal configurations however to comprise the QCA architecture it is needed to electrostatically break the symmetry and polarize the electrons within the cells, this can be obtained by one perturbing charge placed near the cell. Upon charge removal, a rapid tunnel exchange emerges. The resulting coupled SiDB may be described as an artificial homo-nuclear diatomic molecule. Like in an ordinary molecule, the Born-Oppenheimer approximation is valid, so the nuclear motion is much slower than electron motion, the nucleus can be considered to be fixed and is exposed to a smeared-out potential from fast electron motion. This implied that nuclear relaxation does not have time to occur. Placing DBs next to each other such as to electrostatically couple them but preventing tunneling coupling it is possible to control the charge configuration of the QCA cell, and an analog hetero-nuclear diatomic molecule can be obtained. This results in a bond polarization with an ionic character, highlighting the possibility of controlling the electron population of the cell via the applied perturbation even at room temperature. [1]

To obtain different electron localization (thus charge configurations) over the DBs it is also possible to fabricate non-regular QCA cells with appropriate spacing between elements. For example, three neighbors DBs differently spaced give rise to the neutral or negative charge on the central atom varying the spacing of the ensemble: In general, as a rule of thumb wider spaced molecule can host a larger negative charge compared to a tightly spaced molecule. [6]

Finally, both tunnel-coupled atoms and perturbing atoms can be used on the periphery of the ensemble to ensure a local properties change of the individual atoms of the molecule which will be reflected in a change of the whole molecule properties. The great flexibility of this approach allows also for to design of the optical properties of the ensemble, for example modifying the absorption energy or pre-determining absorption modes.[1]

3.4 Operational parameters

Despite the similar surface preparation, variations in physical properties result in different ground state charge configurations for the same DB layout, for example, due to differences in doping level, slight deviations from preparation procedure, and bulk (or surface) defects. These parameters are $\epsilon_r, \lambda_{TF}, \mu_-$ respectively effective surface dielectric constant, Thomas-Fermi screening length and chemical potential which result to be the set of all the band bending effects that contribute equally to all DBs, it can be defined as $\mu_- = E_s - E_F^{Si}$ where E_s is the DB(0/-) transition level and E_F^{Si}. Moreover, it is possible to define a chemical potential for charge transition level DB(0/+) which results be: $\mu_+ = \mu_- - \mathcal{E}$ where $\mathcal{E} = 0.59eV$ potential energy between the +/- charge transition levels. The ground state used for computation results is to be found only for determined ranges of these parameters which can be also tailored by selecting properly the distance between DBs and the distance between the perturber used to feed the circuit. In previous works, it has been found that for the same values of the chemical potential applied to different circuits, the one with a more compact spacing between dots has a wider ϵ_r range acceptable to produce the desirable ground state. This agrees with the guess that more compact circuits prefer to operate under weaker inter-DB interaction that can be tuned with the placements of the dots, this results in a wider operational range for more compact circuits. [6]

Part II

Methodology

Chapter 4

SiDB Modelling

4.1 Coupled Systems

In general 0D systems (QDs) experience a complete quantum confinement of carriers due to their extremely reduced sizes. If we seek a comparison with the traditional CMOS technology and FCN paradigm the reservoir is analogous to the Source/Drain contacts and the QD is related to the channel of the transistor. If we define the escape time, τ as the time interval in which the electron result is to be confined in the dot as:

$$\tau = \frac{\hbar}{\gamma} \tag{4.1}$$

According to the coupling conditions between QDs the interaction among them can be considered:

1. $\tau \to \infty$ there is no coupling between the reservoir and the channel, the dot is considered as a closed system in which electrons are confined indefinitely;

2. $\tau \simeq fs$ the system is in the so-called strong coupling regime or Self-Consistent Field regime where the allowed discrete energy levels of the dot are broadened by the influence of the electrodes, therefore there is an exchange of matter with the external world and the dot can be considered as an open system;

3. $\tau \simeq ns$ the system is in the weak coupling regime (or Coulomb Blockade) regime, corresponding to a weak interaction of the electrodes with the dot, as a result, the energy levels broaden diminish and the electrons result to be more confined in the dot;

We can identify some similarities between the QCA and ASiQDs paradigms: both are planar technologies and exhibit a high device density at a potentially low energy cost, moreover, SiDBs can be populated and depopulated of $e-$ by band bending induced from external biases. In this model, the electron exchange between successive components of the circuit occurs between the surface SiDBs and the silicon bulk which acts as a charge reservoir. Similarly, as three-state zwitterionic molecular QCA when biased, charges move between the +/-1 charge stat and the null, for the SiDB platform, the null state is analogous to the bulk charge reservoir. Due to these similarities, control structures proposed for QCA are compatible with the SiDB framework. [16]

4.2 Methodology

To carry on the analysis of the behavior of SiDB circuits a simplified MoSQuito (Molecular Simulator Quantum-dot cellular automata Torino) methodology has been used, it consists of three main stages[2]:

1. Basic molecule characterization: under the assumption that a SiDB couple can be considered to behave like two coupled dot molecules to examine its electronic structure and physical properties very accurate ab initio simulations based on quantum chemistry are usually carried out. In this work, a simplified model based on the heuristic algorithm for simulated annealing is presented in [1] called SimAnneal is implemented.

2. Post-processing the characterization: the key characteristics, or figures of merit, describing the electrostatic behavior of the molecule are derived from the characterization of the system. These characteristics are then used to delineate interactions with other molecules and extract the quantitative data required for analyzing molecular circuits.

3. System Level Analysis: the MosQuiTo figures of merit established in the second stage allow for the system-level analysis of molecular circuits. The evaluation of the information propagation in MQCA/BDL circuits can take into account factors more closely related to electronic engineering methods in a higher-level approach.

4.3 FCN Figures of Merit

To analyze an FCN circuit it is convenient to define some figure of merits capable of describing the molecular system starting from the basic component of the technology, the characterization of the technology starts with the definition of the Molecule Under Test (MUT) which is considered the minimum SiDB ensemble used in the information propagation in the circuit, every MUT is different according to the number of molecules considered as the basic interacting unit, from this definition it is possible to define the following FOM [14]:

1. Aggregated Charge (AC), as the macroscopic properties of the molecules are of interest is useful to define the sum of all the charges in each dot (i.e. the charge state curves of the DB pair). The aggregated charge distribution is the starting point from which to characterize the electrostatic properties of the MUT;

2. $V_{in} - AC$ Transcharacteristic (VACT): is the correlation between the input voltage and the aggregated charge of the molecule is a $\mathbf{R} \rightarrow \mathbf{R}^N$ where N is the number of

Aggregated Charges describing the MUT. This figure of merit remains unaffected by the receiver molecule's position. Consequently, it can assess the field generated by the MUT when is under the influence of an electric field, enabling the evaluation of interactions between different molecules; [2]

3. Output Voltage V_{out} is the voltage at the receiver, which can be evaluated by integrating the electric field on the segment that connects active dots.

Usually, active molecules can be classified concerning the final charge occupation they present after the interaction with other chemical species:

1. Oxidized molecules, characterized by the loss of electrons due to interactions with other species, these molecules have a net free positive charge (i.e. having $AC_{D_1} + AC_{D_2} = +1$);

2. Reduced molecules, characterized by the gain of electrons due to interactions with other species, these molecules have a net free negative charge (i.e. the AC in the VACT is $AC_{D_1} + AC_{D_2} = -1$). An example of reduced VACT is presented in 4.1 it is a transcharacteristic already present and available in the SCERPA database;

3. Neutral molecules, characterized by a net neutral charge the sum of the aggregated charge over the two dots is $AC_{D_1} + AC_{D_2} = 0$.

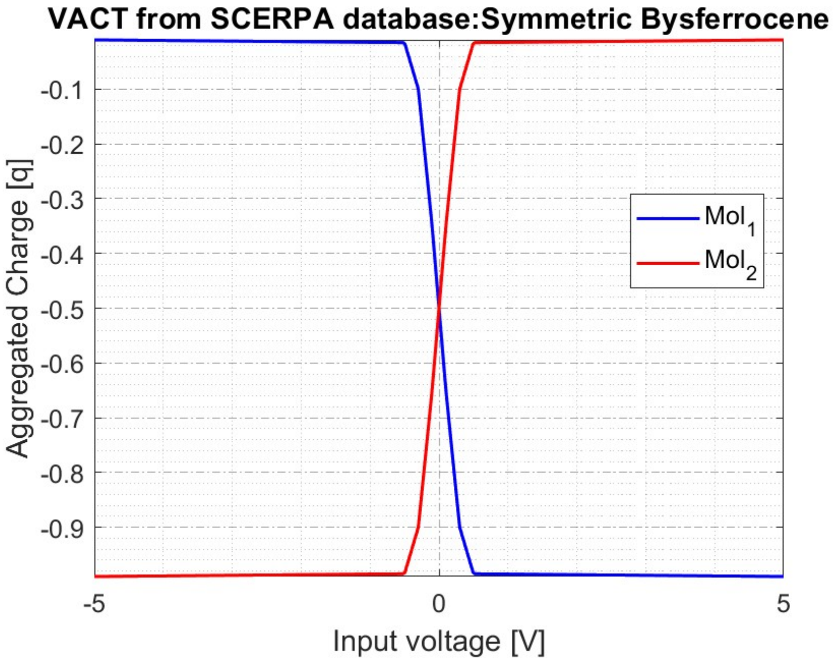

Figure 4.1: Example of reduced VACT obtained from the symmetric Bisferrocene [2][3] molecule already available in the database included in SCERPA.

Thus depending on the available net free charge the molecule will assume the relative oxidation state. The DBs couple can be considered to be a neutral molecule when the dots are placed very far one concerning the other that represents the condition until the Self-Biasing effect arises. When the distance of the two dots is sufficient to expel the fourth electron in the bulk (SBE) we can consider To ensure the distinguishability of the logic states a certain charge separation between the active dots must be ensured, thus thinking of the MUT as a reduced/oxidized or neutral molecule we can classify it into three categories depending on the electron occupation versus the electron occupation at the equilibrium of the single dots in:

The SiDB pair can contain a maximum of three electrons due to self-biasing (SB), whereas a single DB's orbitals could contain two electrons each. However, an adjacent pair of DB assumes a ground state in which the excess electron is in a metastable state on the leftmost DB, so the leftmost has a negative charge because it hosts the metastable electron, while the rightmost DB has a positive charge finally leading having a net neutral charge. This is achieved by considering the DB ensemble to be made up of single DBs, whereas if we were to think of the pair as an interacting molecule, it would host three electrons due to the SBE, losing in the bulk the fourth electron that neutralizes the charge, causing the ensemble to be oxidized or equivalently reduced (depending on the carrier which is used in the application) rather than neutral.

Chapter 5

SCERPA: Self-Consistent Electrostatic Potential Algorithm

To address the problem of the too-high computational costs of ab initio calculations for analyzing information propagation in more complex FCN circuits it is possible to exploit SCERPA, a self-consistent electrostatic potential algorithm capable of evaluating the information propagation among molecular circuits using an iterative procedure.

To model the influence over the MUT define a test charge q^t the one in a generic point of the space of which electric field effect over the MUT is needed, consider as q^1 the charge of one dot separated by a distance $\mathbf{r_1}$:

$$\mathbf{r_1} = \sqrt{(x-x_0)^2 + (y-y_0)^2 + (z-z_0)^2} \quad \hat{r}_1 = r_1\hat{r} \tag{5.1}$$

Taking into account the reference system presented in 5.1 the electric field $\mathcal{E}(x,y,z)$ influencing the q^t dot due to q^1 combining Coulomb force and Gauss law can be expressed as:

$$\mathcal{E}_{\mathbf{1}} = \frac{\mathbf{F}_1}{q^t} = \frac{q^1}{4\pi\epsilon_0 r_1^2} \tag{5.2}$$

From which adding all available charges in the space the following is obtained:

$$\mathcal{E}_{\mathbf{TOT}} = \frac{\mathbf{F}_{TOT}}{q^t} = \sum_{i=1}^{N} \frac{1}{4\pi\epsilon_0} \frac{q_i}{r_i^2}\hat{\mathbf{r}} \tag{5.3}$$

The generation of the q_i charges can be associated either with aggregated charges or to all atoms resulting in more precise and more computational expansive.

The driver electric field generates a V_{in} in the MUT that as a consequence will exert an electric field over the following one, placing molecule after molecule the information under the form of a V_{in} is lost the last propagating molecule have not sufficient energy to switch allowing information to fade.

Having a generic number of dots the info propagation can be addressed by solving a self-consistent problem inherent to the input voltage at each molecule which depends on the electric field of the previous neighbor which in turn depends on the V_{in} induced by the driver that is fixed and user-controlled. Denoting as $d(\mathbf{r}_A, \mathbf{r}_B)$ the Euclidean distance between two points $\vec{r}_A$ and $\mathbf{r}_B$, assuming that a set of N_{AC} aggregated charges, $\{Q_D^1, \ldots, Q_D^N\}$, in the positions $\{\mathbf{r}_D^1, \ldots, \mathbf{r}_D^N\}$ represents the driver molecule, the voltage produced by the driver $\mathbf{V}_D$ at an arbitrary point of 3-D space $\mathbf{r}$ can be found as: [14]

$$\mathbf{V}_D(\mathbf{r}) = \frac{1}{4\pi\epsilon_0} \sum_{\beta=1}^{N} \frac{Q_i^D}{d(\mathbf{r}_\beta^D, \mathbf{r})}, \tag{5.4}$$

where ϵ_0 is the vacuum permittivity. Therefore, if $\mathbf{r}_{MUT_1}$ and $\mathbf{r}_{MUT_2}$ are the positions of the Dot_1 and Dot_2 of the MUT, the impact of the driver over the molecule can be addressed as a voltage difference between the two active dots:

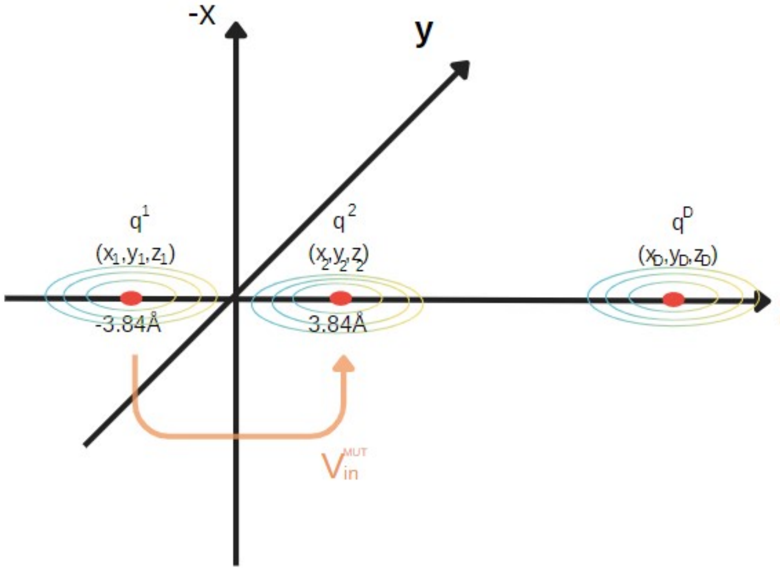

Figure 5.1: Electrostatic definition of the SiDB couple in the SCERPA's reference system, the basic couple represented was used as the building block for more complex circuits, to simulate more complex circuits having blocks of more than two molecules it is needed to define a new VACT contemplating more than two components.

$$\mathbf{V}_{D,\mathrm{MUT}} = \int_{\mathbf{r}_{\mathrm{MUT}_1}}^{\mathbf{r}_{\mathrm{MUT}_2}} \mathbf{E}_D \cdot d\mathbf{l} = \mathbf{V}_D(\mathbf{r}_{\mathrm{MUT}_2}) - \mathbf{V}_D(\mathbf{r}_{\mathrm{MUT}_1}), \tag{5.5}$$

where $\mathbf{E}_D$ is the electric field generated by the driver molecule charge distribution. Considering as input voltage $\mathbf{V}_{D,\mathrm{MUT}}$, the aggregated charges of the molecules are obtained by applying the transcharacteristics obtained in the first step. This makes it possible to evaluate how molecule reacts to adjacent components resulting in intermolecular interaction which is ultimately related to the information propagation in a molecular circuit.[14]

Consider a generic molecular wire, the $j-th$ Molecule can be modeled as a set of N_{AC} charges, $\{Q_{j1},\ldots,Q_{jN_{AC}}\}$, placed at $\{r_{j1},\ldots,r_{jN_{AC}}\}$ in the 3-D space. The voltage generated by Molecule j at a generic point $\mathbf{r}$ in the 3-D space can be evaluated as the driver-induced voltage:

$$\mathbf{V}_j(\mathbf{r}) = \frac{1}{4\pi\epsilon_0}\sum_{\beta=1}^{N_{AC}}\frac{Q_\beta^j}{d(\mathbf{r}_\beta^j,\mathbf{r})}, \tag{5.6}$$

The molecule j affects all the molecules in the wire along both the input and output directions. Modelling a second generic Molecule i with the aggregated charges $\{Q_{i1},\ldots,Q_{N_{AC}}^i\}$ at positions $\{r_1^i,\ldots,r_{N_{AC}}^i\}$ it is possible to assess the voltage that the molecule j exerts over the molecule i:

$$V_{j,i} = V_j(\mathbf{r}_i) - V_j(\mathbf{r}_j) = \frac{1}{4\pi\epsilon_0}\sum_{\beta=1}^{N_{AC}}\left[Q_\beta^j\left(\frac{1}{d(\mathbf{r}_1^i,\mathbf{r}_\beta^j)} - \frac{1}{d(\mathbf{r}_2^i,\mathbf{r}_\beta^j)}\right)\right], \tag{5.7}$$

Once the Molecule i is influenced by Molecule j it can be also considered as a driver that applies its feedback effect to all other molecules. Having a set of N molecules in the wire, the input voltage $V_{in,i}$ for Molecule i is assessed, considering the effects of the driver $V_{D,i}$ and all other molecules $V_{j,i}$. The problem can be finally formalized as a non-linear system by introducing the molecules' transcharacteristics, where the aggregated charges of Molecule j rely on $V_{in,j}$. The transcharacteristics are also influenced by the clock value applied to the circuit for implementing adiabatic propagation and allow information flow through clock phases:

$$V_{in,i} = V_{D,i} + \sum_{j=1,j\neq i}^{N} V_{j,i}(V_{in,j}, E_{\mathrm{clk},j}), \tag{5.8}$$

The value of the clock field E_{clk} is known and user-defined. The algorithm supposes an initial input voltage for all the molecules and then iteratively applies the previous equation to determine the approximated solution of the non-linear system depending on all the input voltages of all the molecules:

$$V_{\mathrm{in},i}^k = V_{in,i}(V_{\mathrm{in},1}^{k-1},\ldots,V_{\mathrm{in},i-1}^{k-1},V_{\mathrm{in},i+1}^{k-1},\ldots,V_{\mathrm{in},N}^{k-1}) \tag{5.9}$$

k is the single step of the iterative procedure. [14]

SiDBs with specific geometric and physical parameters can be strongly coupled with the neighbors and their electrodes. Moreover given that the tunneling period between SiDBs is of the order of around 10 femtoseconds it is feasible to exploit the self-consistent field regime to simulate the behavior of more complex DB circuits using SCERPA.

Chapter 6

Modelling atomic Silicon quantum dots

6.1 Interaction model of a two SiDB molecule

At first, to be able to understand the behavior of a SiDB ensemble with the self-consistent algorithm, the heuristic annealing introduced by Ng et al in [6], a code mimicking the SiQAD [6] algorithm has been prepared, it was able to predict the behavior of a SiDB couple taking advantage of the parameters and the methodology introduced in [6]. This approach aimed to understand how to generate trans-characteristic that SCERPA could use to simulate more complex circuits. The geometric layout presented in 6.1 was used as an arrangement for the Fermi statistic approach that defined the charge transfer between SiDBs in the basic couple ensemble.

The external perturbation has been fed to the system via an external voltage modeled with a third DB acting as a perturber. [16] [6] The electrostatic interactions among different DBs have been modeled with a screened Coulomb potential as discussed in [16] [6] [4]. This approach even if not a proper ab initio simulation represents a good approximation for the electrostatic interaction between DBs charges:

$$Vij = -\frac{q}{4\pi\epsilon_r\epsilon_0} \cdot \frac{1}{r_{ij}} \cdot e^{-\frac{r_{ij}}{\lambda_{TF}}}; \tag{6.1}$$

where r_{ij} the distance between the DBs, λ_{TF} the Thomas-Fermi screening length, ϵ_0 ϵ_r respectively the vacuum permittivity and the effective dielectric constant at the surface and r_{ij} is the distance between the two dots. All these parameters have been taken from the possible values presented in [6] and can be user-tuned.

By using the Coulomb potential, it is possible to quantitatively assess the interaction between charged DBs and other charges on the substrate, such as carriers or defects. This approach allows to investigate the charge distribution that can be identified with the calculation of the energy ground state of the system. Later on, a Lennard-Jones potential was added to take into account the van der Waals and short-range interactions among atoms adding a layer of accuracy to the inter-DB potential calculation but increasing

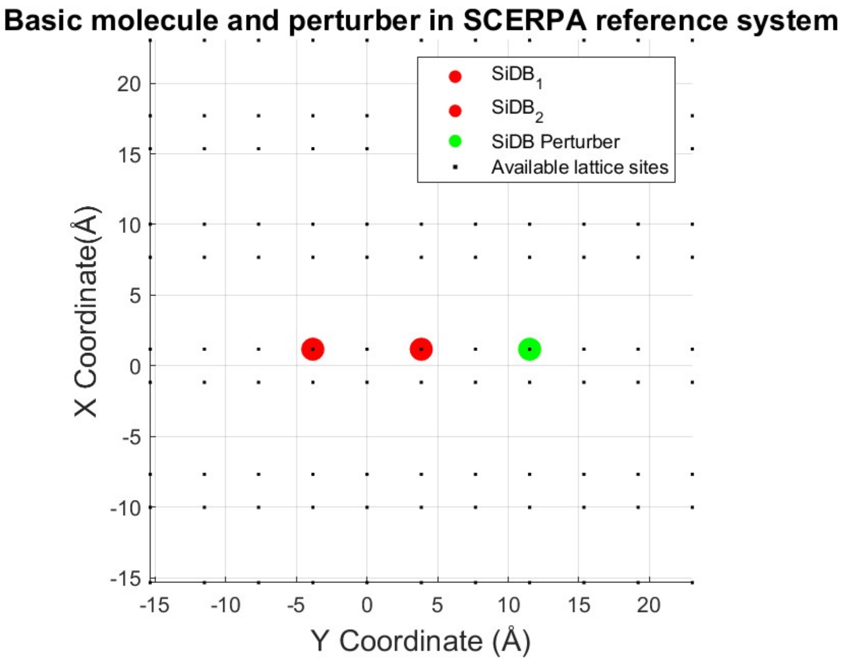

Figure 6.1: SiDB couple used as a base molecule for SCERPA calculations, the perturber was not included in the molecule as it was fictitious, to simulate the behavior of a forcing external potential.

the computational cost of the algorithm which can result in being too expansive while increasing the DB number:

$$V_{LJ} = 4 \cdot (2U_0) \cdot \left(\left(\frac{l_{x_1}}{r_{ij}} \right)^{12} - \left(\frac{l_{x_1}}{r_{ij}} \right)^{6} \right) \tag{6.2}$$

Where l_{x_1} is the distance in which the minimum of the potential well lies and U_0 is the depth of the potential well which was taken to be the Si-H band gap that is 1.1eV. Finally, the potential at each DB has been obtained as:

$$V_i = -V_i^{ext} - \sum_j (V_{ij} + V_{LJ}) q_j \tag{6.3}$$

The results for these potential calculations have been found in good agreement with the experimental result for the same geometry presented in [6].

To find the more stable charge configuration the energy ground state has been extracted as the minimum among all the possible energies arising from the combination of possible charge states:

$$E(\vec{n}) = \sum_i V_i^{ext} q_i + \sum_{i<j} V_{ij} q_i q_j \tag{6.4}$$

Where V_i^{ext} is the total external potential fed to the i-th DB excluding the interactions with neighboring DBs, $q_{i/j}$ is the charge state of each DB with possible values $q_i \in \{-1, 0, +1\}$which are the $\{DB^-, DB^0, DB^+\}$ charge states. The V^{ext} has been modeled with a potential similar to the interaction between DBs, thus like a fixed perturber placed at a given distance from the interacting DBs:

$$V_i^{ext} = V^{ext}\frac{q}{4\pi\epsilon_r\epsilon_0}\frac{1}{r_{pert,i}}e^{-\frac{r_{pert,i}}{l_{TF}}} + 4V^{ext}\cdot(2U_0)\left(\left(\frac{l_{x_1}}{r_{pert,i}}\right)^{12} - \left(\frac{l_{x_1}}{r_{pert,i}}\right)^{6}\right) \tag{6.5}$$

V_{ij} is the strength of the Coulombic interaction between DBs as previously defined and $r_{pert,i}$ is the distance of the fixed DB used as perturber exploited to calculate the interaction between the two components. While V^{ext} is an artificial external voltage used to span over the probability calculation.

The interest in calculating the potentials and the charge configuration was to generate a VACT curve that closely represents the occupied e^-/h^+ states thus a charge transition model for determined input voltages. To finally obtain this curve, given that only one electron (or hole) transition can occur inside a closely-spaced couple, the probability of having an e^-/h^+ transit from a DB to the other was used to obtain the total charge available for the actual computing process. With this approach only the transition probabilities were needed, thus exploiting the Fermi statistics the total aggregated charge for a single DB resulted to coincide with the difference between positive and negative transitions:

$$Q_{Tot}^{DB_i} = -\mathcal{P}_{0\to-1}^{DB_i} + \mathcal{P}_{-1\to0}^{DB_i} \tag{6.6}$$

where the probabilities of the negative and positive transitions have been calculated as a Fermi-Dirac distribution in which the potential, V_{ov} is the override potential which represents the total band bending that is fed to the i-th DB, $\mathcal{P}_{-1\to0}$ represents the chance that an electron has to be bounced back to the bulk from the i-th DB and vice versa, the positive transitions are always null while the negative transitions which refers to excess electrons in 6.2 6.3 give to the AC its trend:

$$\mathcal{P}_{0\to-1}^{DB_i}(V_{ov}) = \frac{1}{1+e^{\frac{V_{ov}}{k_BT}}} \quad \text{where} \quad V_{ov} = -q_i(V_i+\mu_i) \tag{6.7}$$

$$\mathcal{P}_{-1\to0}^{DB_i}(V_{ov}) = \frac{1}{1+e^{\frac{V_{ov}}{k_BT}}} \quad \text{where} \quad V_{ov} = q_i(V_i+\mu_i) \tag{6.8}$$

the V_{ov} is the override potential, the total band bending fed to the corresponding element of a molecule. Moreover, it can be noticed that:

$$\mathcal{P}_{-1\to0}^{DB_i}(V_{ov}) = 1 - \mathcal{P}_{0\to-1}^{DB_i}(V_{ov}) \tag{6.9}$$

Due to the ability of SiDBs to exhibit both a neutral, reduced, and oxidized behavior, it was needed to manipulate the charge to obtain a molecule exhibiting a reduced behavior which was found to be more consistent with the technological usage of carriers in electronic devices' history, the result of this operations were found to be the reduced

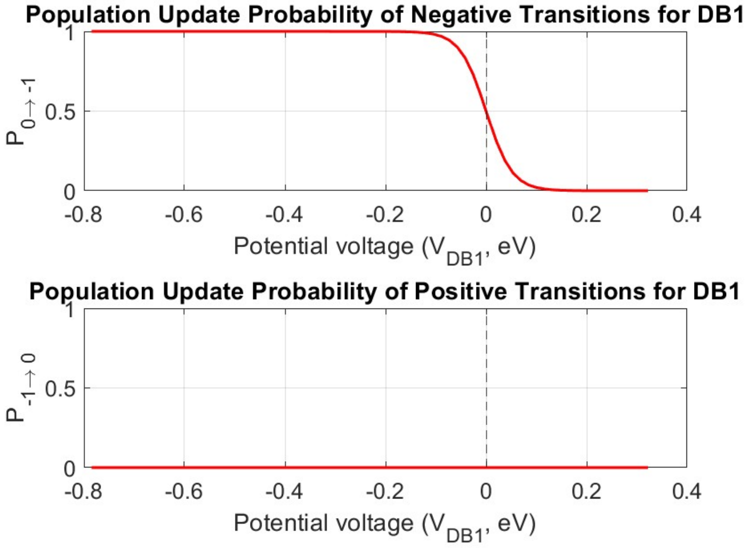

Figure 6.2: Positive and negative transition probabilities for the DB_1 having the perturber placed at $2 \cdot 7.68$Åaway from it, leading to a weaker external potential concerning its neighbor.

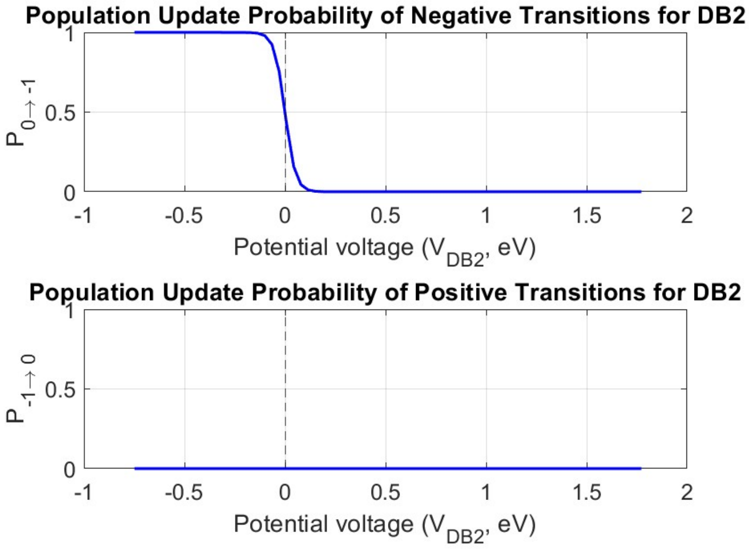

Figure 6.3: Positive and negative transition probabilities for the DB_2 having a perturber placed at 7.68Å from it, leading to a stronger external potential acting on the second dot.

transcharacteristic presented in 6.4. Still, it is up to the user and relatable to the device application to choose the electrons or holes as carriers because their behavior is still

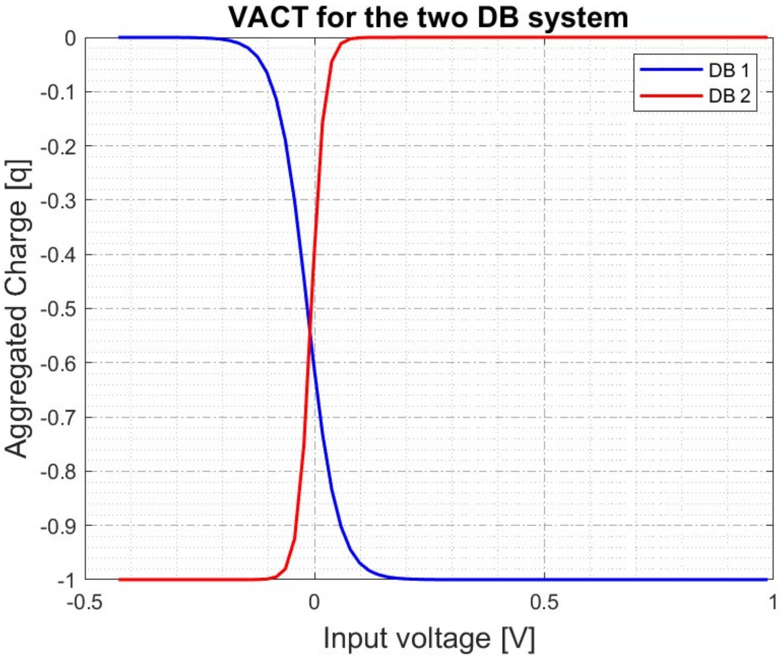

Figure 6.4: VACT obtained from an interaction model supposing that the molecule identified as the SiDB couple is a reduced molecule that shares with the environment one electron.

completely symmetrical. The calculation of the VACT concludes the preparation of the self-consistent algorithm, the input voltage has been taken as the difference of the override potential voltages of each DB without taking into account the charge state, to remain consistent with the definition of the input voltage of the trans-characteristic:

$$V_{in} = \frac{V_{ov}}{n_1} + \frac{V_{ov}}{n_2} \tag{6.10}$$

where $n_1$andn_2 are the charge state of the corresponding DB taken from the annealing results.

6.2 SCERPA simulations

The ground state simulator is used to feed the self-consistent algorithm with the VACT and the layout of the basic SiDB molecule, thus substituting the first stage of the MosQuiTo methodology. Once the VACT and the geometric layout have been set the electric field can be computed at any point of the space surrounding the molecules with electrostatic equations.

6.2.1 SiDB binary dotted logic wire

Considering the reference system of SCERPA the two-DB system gets as coordinates for the simple horizontal couple: $r_{DB_1} = (0, 0, -3.84)$Åand $r_{DB_2} = (0, 0, +3.84)$Å. Adding the layout of a binary dotted logic wire like the one in 6.5 the earlier obtained transcharacteristic have been used in the self-consistent potential algorithm to simulate its electrostatic behavior. To be able to validate the results obtained with SCERPA the results in [4] have been taken as a yardstick; to be able to compare them the layout of the wire in SCERPA is the same in [4]: each couple is separated by $5 \cdot 3.84$Åand a driver representing the perturber is placed on the right or the left of the circuit depending on the need to have a logic 0 or 1 as an input, so two simulations were needed to be able to model the different layout of the input signals.

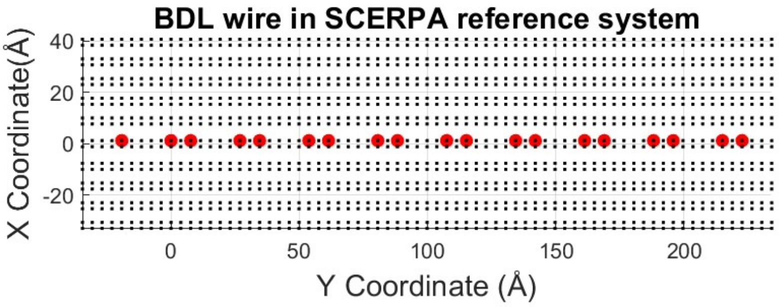

Figure 6.5: Example of BDL wire having the perturber placed on the left which is used to impose a logical 1, placing the perturber on the right is useful to establish the logic 0 over the circuit.

Due to how the information is encoded for this technology, to push the charge to assume a certain configuration over the wire a DB with a fixed charge state called perturber is placed at the beginning of the wire on both the left or right depending on the input that should be imposed, and its distance with respect to the first propagating molecule is used to encode the 0/1 information propagation. To translate into SCERPA the perturber a SiDB molecule with VACT equal to the VACT of the circuit's components was first used, with the awareness that it didn't represent a single atom but a couple of DB having an aggregated charge located over the first or second dot depending on the input voltage.

At first, a two-phase simulation was exploited but it required running two times the self-consistent algorithm to obtain the two possible input states for a single driver. To be able to simulate all the input and output combinations for a driver in a given layout, the structure of the simulation has been set as a four-phase signal in which the odd phases are used to reset the system and give enough time to the molecules to follow the driver charge switching and change charge configuration as consequence. This approach allowed obtaining a driver that presented the charge near to the first DB of the wire or away from it thus simulating the choice of having a negatively charged dot close or away from the propagating molecules. So for the left and right perturber positions used to propagate respectively the 1 and 0 input signal the four phases gave as a result of the propagation the following outcome, presented with three of the most important figures of merits that SCERPA is calculating by default:

- The 1D charge along the wire (available for 1D structures only) is a representation of how the charge is arranged along the dots of the molecules belonging to the wire;
- The potential over the circuit, where the excess electron on a dot is represented with a dark dot while the presence of a hole is represented with a bright dot;
- The 3D ball-stick model of the charge distribution along the wire.

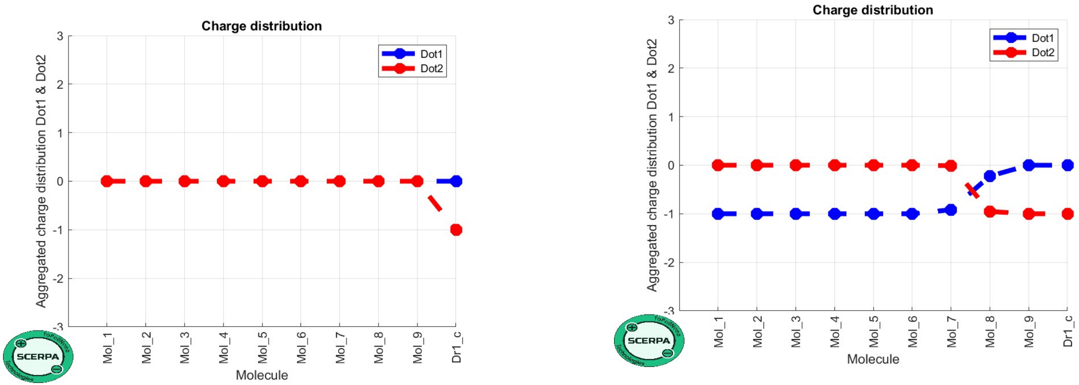

(a) First phase of the driver input corresponding to a reset state

(b) Second phase of the driver which after the reset is pushing an input state corresponding to a logical 1

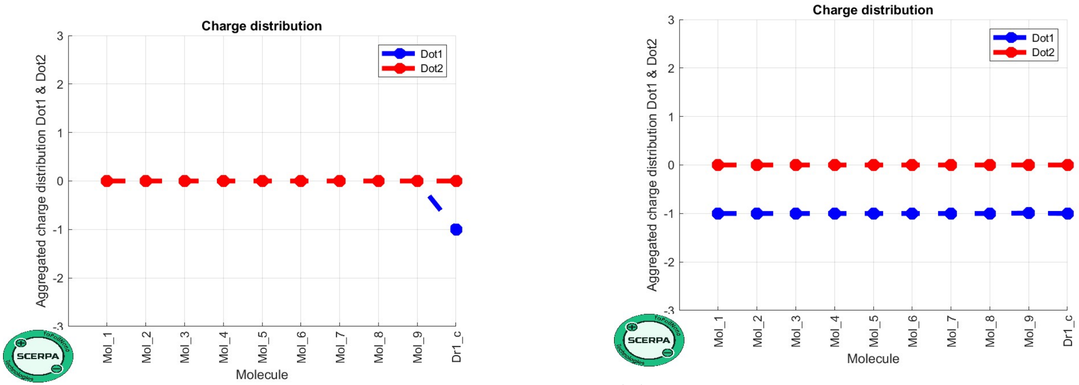

(c) Third phase used as reset to let the circuit be able to adjust itself and follow the second input

(d) Fourth phase corresponding to a logical 0, after the reset time the driver was capable of pushing the charge in the correct direction

Figure 6.6: 1D aggregated charges over the SiDB couples, already from comparing these figures with the experimental results presented in [4] the mixed signal configuration is not correct, missing the expected symmetry deriving from having a driver which behaves like a molecule of the circuit having it the same VACT of its neighbors.

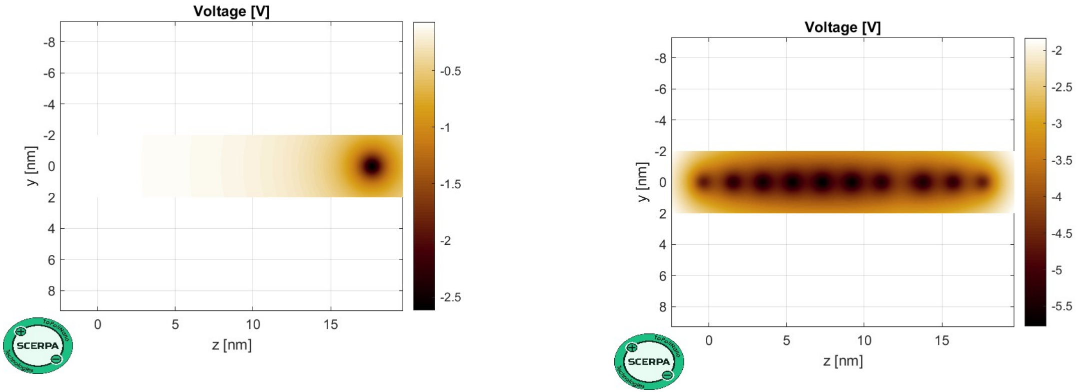

(a) Electrical potential of the first phase of the driver input corresponding to a reset state

(b) Second phase corresponding to the 1 signal

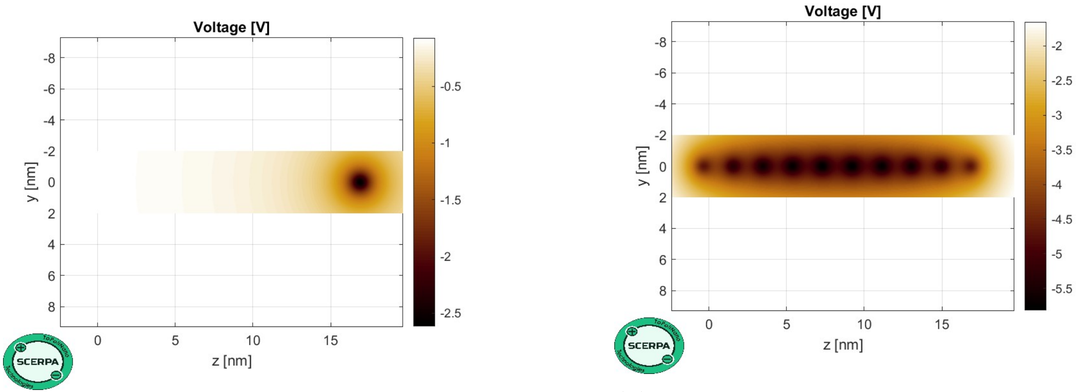

(c) Third phase used as reset to let the circuit be able to adjust itself and follow the second input

(d) Fourth phase corresponding to a logical 0, after the reset time the driver was capable of pushing the charge in the correct direction

Figure 6.7: The electrical potential is indicative of the charge state given as a result of the VACT used as a model for the molecules and the circuit's layout simulating a virtual tip placed at 5.5Åfrom the surface.

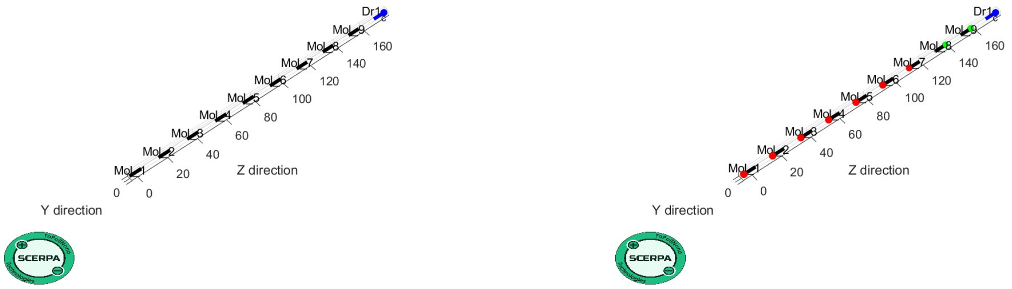

(a) First phase of the driver input corresponding to a reset state

(b) Second phase of the input driver which after the reset is pushing a 1 across the wire

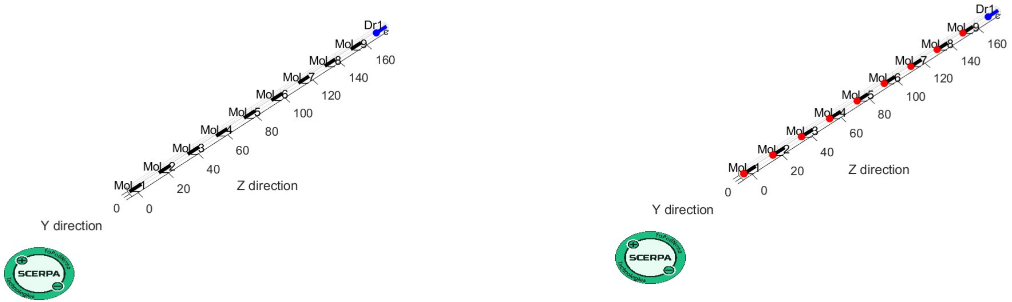

(c) Third phase used as reset to let the circuit be able to adjust itself and follow the second input

(d) Fourth phase corresponding to a logical zero, after the reset time the driver was capable of pushing the charge in the correct direction

Figure 6.8: 3D ball and stick model of the wire's charge configuration, it is clear comparing this result with the experimental results presented in [4] that the mixed signal configuration is not correct having the sixth and seventh couple in the opposite charge configuration with respect the expected ones.

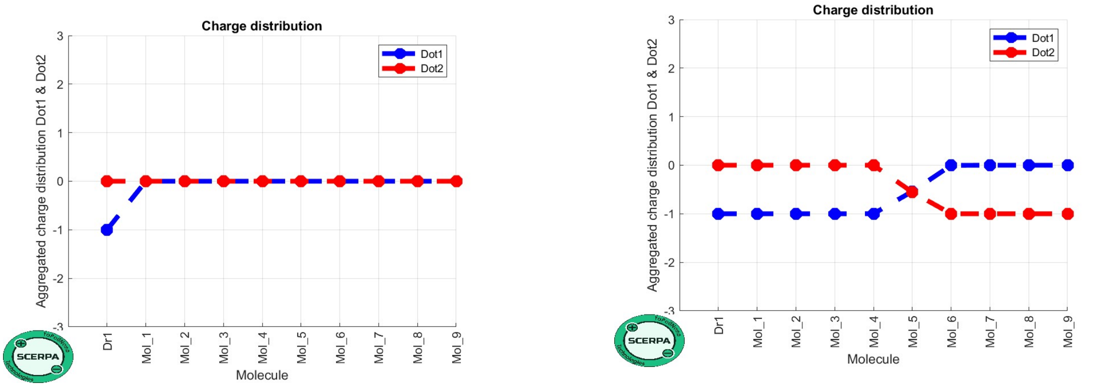

(a) First phase of the driver input corresponding to a reset state

(b) Second phase of the driver which after the reset is pushing an input state corresponding to a logical 1

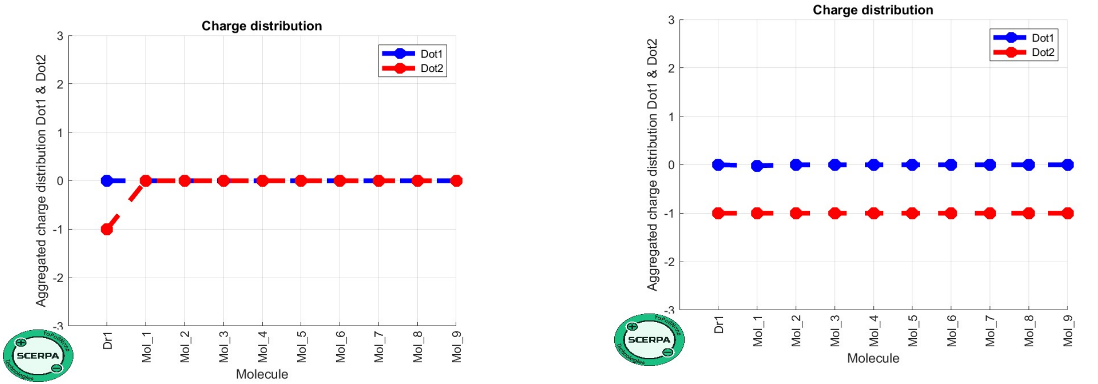

(c) Third phase used as reset to let the circuit be able to adjust itself and follow the second input

(d) Fourth phase corresponding to a logical 0, after the reset time the driver was capable of pushing the charge in the correct direction

Figure 6.9: The 1 signal at the left of the wire correctly propagates, despite the incorrect placement of the charge along the driver, it is still able to push the charge in the right direction and able to propagate at the end of the wire.

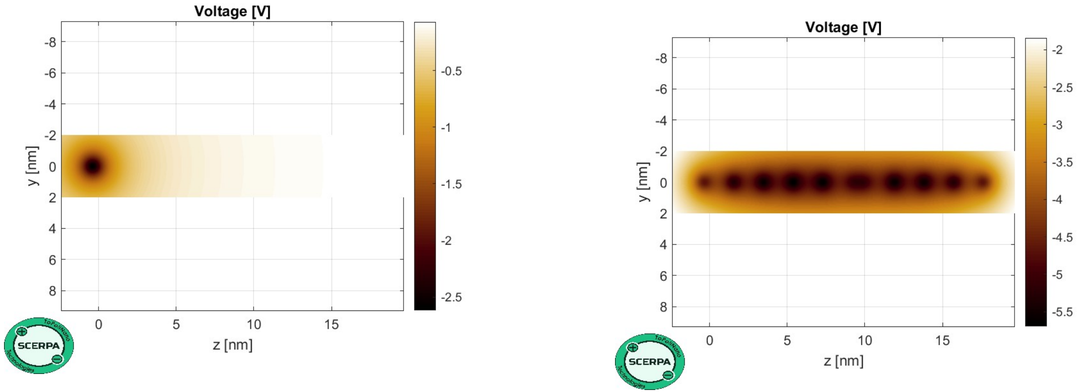

(a) Electrical potential of the first phase of the driver input corresponding to a reset state

(b) Second phase corresponding to the 1 signal

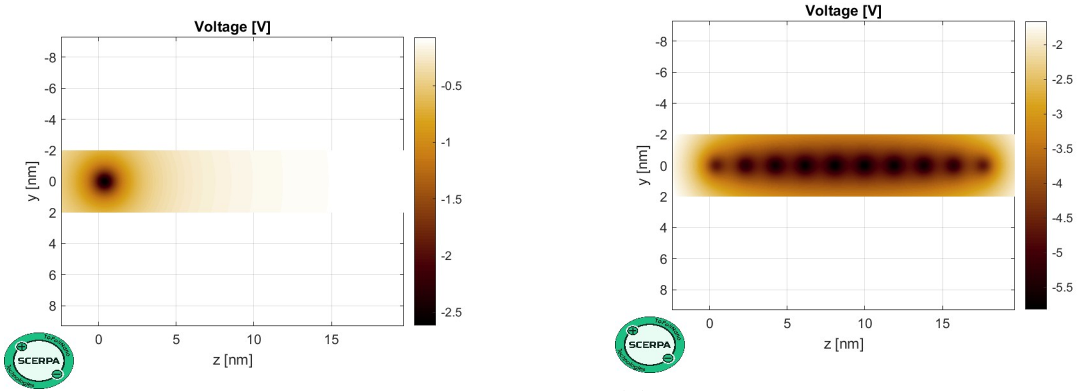

(c) Third phase used as reset to let the circuit be able to adjust itself and follow the second input

(d) Fourth phase corresponding to a logical 0, after the reset time the driver was capable of pushing the charge in the correct direction

Figure 6.10: The electrical potential is indicative of the charge state given as a result of the VACT used as a model for the molecules and the circuit's layout simulating a virtual tip placed at 5.5 Åaway from the surface.

(a) First phase of the driver input corresponding to a reset state

(b) Second phase of the input driver which after the reset is pushing a 1 across the wire

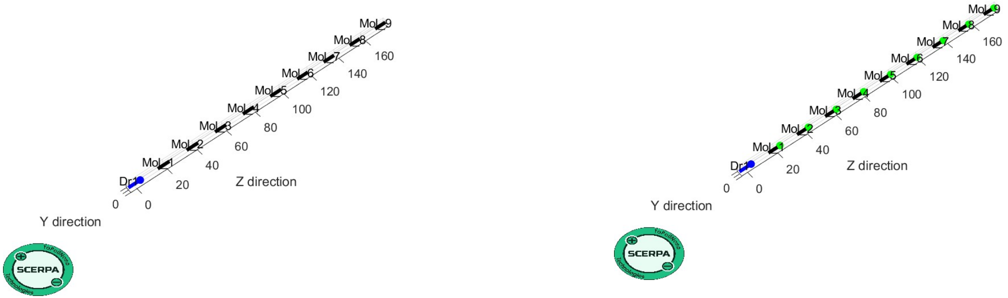

(c) Third phase used as reset to let the circuit be able to adjust itself and follow the second input

(d) Fourth phase corresponding to a logical zero, after the reset time the driver was capable of pushing the charge in the correct direction

Figure 6.11: 3D ball-stick model of the 1 signal propagating from the left to the right of the circuit.

Comparing the results of the simulations with the experimental evidence presented in [4], it is clear that the electrostatic of the wire simulated using the basic reduced molecule as perturber is not propagating the correct information when the AC of the driver is placed away from the first propagating molecule. From 6.9b compared with 6.9b the wire follows the correct charge configuration only when it is naturally forced to, from the first we see that the driver controls only the first half of the circuit while the second half does not propagate correctly the information, in the second figure this does not occur because, on that side of the wire, the charge is capable of naturally assume the needed charge configuration. From the 1D charge configurations in 6.6 6.9 we have first information on how the charge propagates along the wire while from the 3D charge models in 6.8 6.11 we get information on how the charge is displaced along the wire independently from the carriers involved which in turn can be found in the potential images like 6.18 6.7, here the holes and electrons are differently represented indeed AFM images-like are presented, e^-

have a black hue while holes are represented as bright spots.

The presented results highlighted the need to revisit the perturber definition to more closely represent the real single-atom SiDB exploited in the experimental evidence since the reduced VACT used for the molecules relied on the distance between the driver's charge and the first molecule of the system to represent the 0/1 info propagation. To simulate with SCERPA a driver that can be assumed to be similar to a single dot molecule a new VACT was defined as having only one active dot which is chosen with respect to the vicinity of the dot with respect to the propagating molecules of the wire and the charge embedded in the perturber: a positive charge was used to model a 0 while a negative charge was used to propagate a 1.

6.2.2 Towards the modeling of a perturber

Being SCERPA a molecular simulator, to be able to simulate a single atom acting as a driver it needed to have the characteristic to exhibit both the DB^{+}/DB^{-} and DB^{0} charge states and force the circuit to push the charge along the wire depending on the position with respect the rest of the molecules. This can be obtained by setting to zero the AC of the selected DB as presented in 6.12 6.13.

To get nearer to the real atomic SiDB behavior an adjusting over the driver's VACT was needed, to make it more similar to a single atom, a molecule capable of assuming the +/-1 charge state and able to push a 0/1 signal depending on the charge position on its dots with respect the wire direction was needed. To reach such a goal a driver having a reduced/oxidized characteristic depending on the voltage sign was used, such a VACT can simulate the presence of a perturber having DB^{-} charge state corresponding to a reduced dot, and a DB^{+}, corresponding to an oxidized dot, so depending on the position of the driver the oxidized state is capable of pushing a 0 while the reduced state is capable of pushing a 1 and the dot of the basic molecule on which this happens allows the wire to assume or not the correct charge layout, for example having a driver placed on the left of the circuit the VACT should be as in 6.13 to push a logical 1 across the wire, thus the first dot of the second molecule results to be excited and the charge in the circuit propagates correctly. The exact opposite should be considered to obtain a logical 0 on the right of the circuit (to have a distinguishable logic we need to define a 0 and a 1 propagating signal) thus as in fig.6.12 the oxidized part of the VACT should push the signal, so referring to the results as obtained with $VACT_1$ and $VACT_2$:

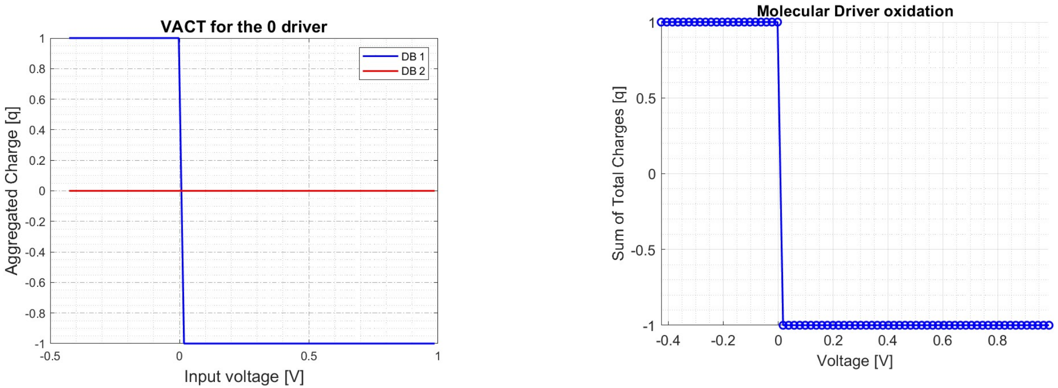

(a) $VACT_1$ of the driver used as logical 0 on the right of the wire

(b) Oxidation of the driver used for the logical 0 depending on the charge of the input voltage

Figure 6.12: $VACT_1$ representing a perturber through a molecule having an oxidized characteristic for negative input voltage and reduced characteristic for positive input voltage. Using such a perturber the system correctly simulates a single atom acting as a perturber over the system, with this representation the driver has two possible charge states as the real perturber exploited to push the correct charge through the wire.

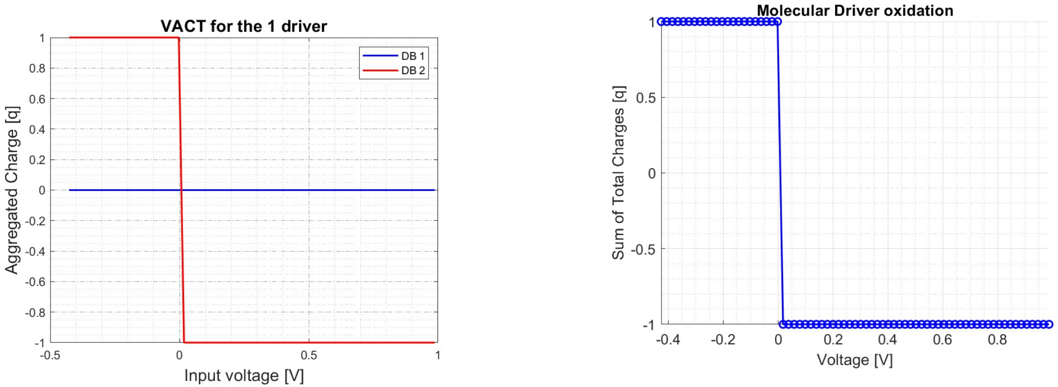

(a) $VACT_1$: the driver used as logical 1 on the left of the wire

(b) Oxidation of the driver used for the logical 1 depending on the charge of the used input voltage

Figure 6.13: $VACT_2$ representing a perturber through a molecule having an oxidized characteristic for negative input voltage and reduced characteristic for positive input voltage. The difference with respect the 0 is the DB in which the charge is located, due to electrostatic considerations the driver's dot in which the charge changes has to be the one nearest to the first component of the circuit otherwise the signal cannot be propagated correctly along the whole wire.

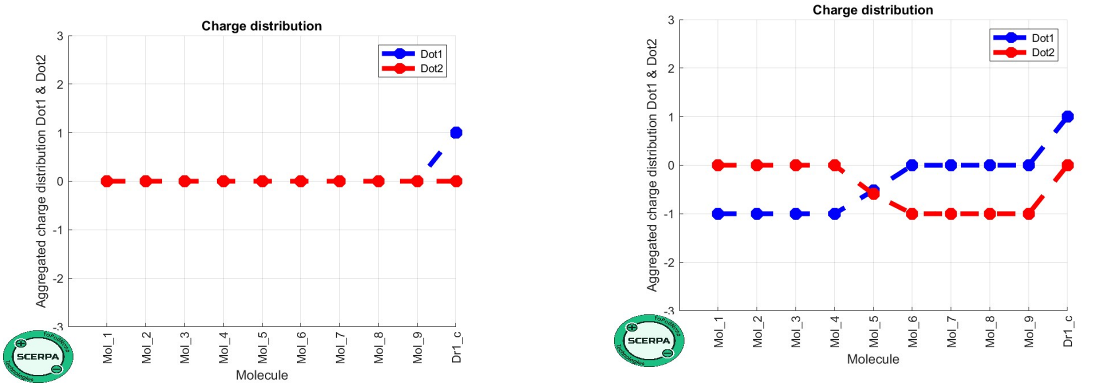

(a) First phase of the driver input corresponding to a reset state

(b) Second phase of the driver which after the reset is pushing an input state corresponding to a logical 1

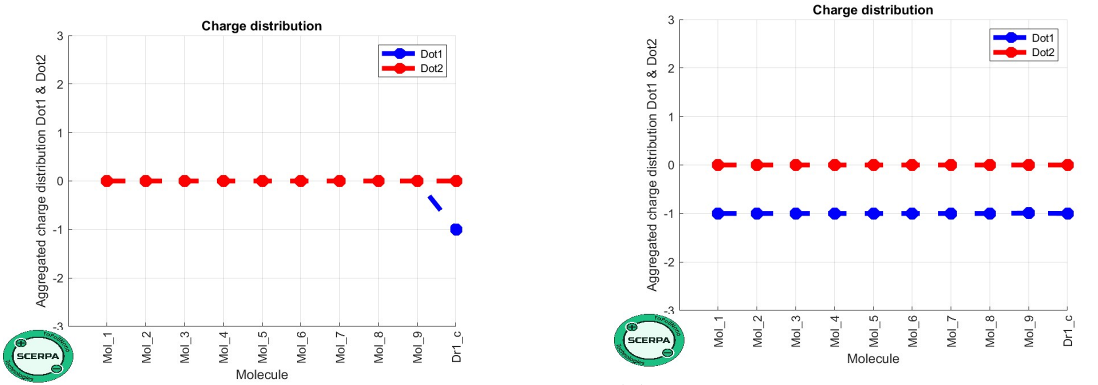

(c) Third phase used as reset to let the circuit be able to adjust itself and follow the second input

(d) Fourth phase corresponding to a logical 0, after the reset time the driver was capable of pushing the charge in the correct direction

Figure 6.14: $VACT_1$: 1D aggregated charges over the SiDB couples, the metastability over the second molecule is not expected and should not be present due to the fact that the number of couples is not even, thus the expected aggregated charge in the middle couple is the dot_1 occupied and the dot_2 unoccupied.

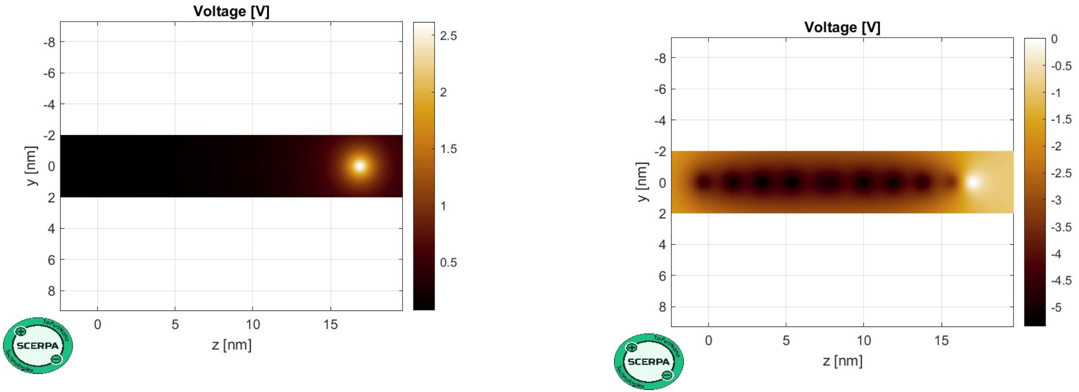

(a) Electrical potential of the first phase of the driver input corresponding to a reset state

(b) Second phase corresponding to the 1 signal

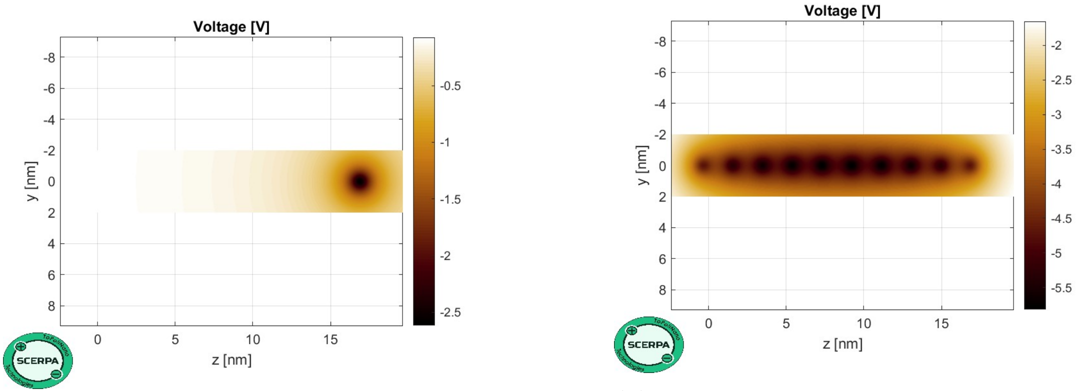

(c) Third phase used as reset to let the circuit be able to adjust itself and follow the second input

(d) Fourth phase corresponding to a logical 0, after the reset time the driver was capable of pushing the charge in the correct direction

Figure 6.15: $VACT_1$: The electrical potential is indicative of the charge state given as a result of the VACT used as a model for the molecules and the circuit's layout simulating a virtual tip placed at 5.5Åfrom the surface.

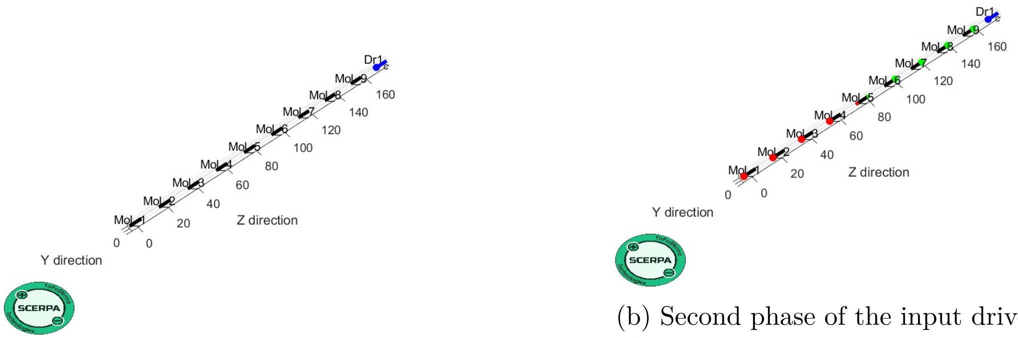

(a) First phase of the driver input corresponding to a reset state

(b) Second phase of the input driver which after the reset is pushing a 1 across the wire, it can be seen that the direction in which the charge is pushed is the opposite with respect to the driver's charge configuration.

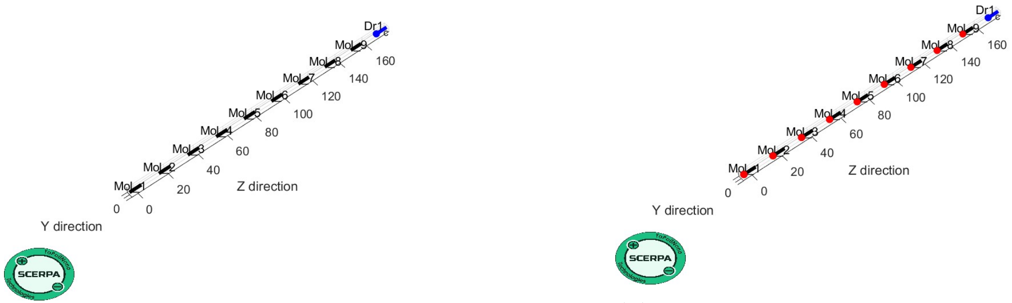

(c) Third phase used as reset to let the circuit be able to adjust itself and follow the second input

(d) Fourth phase corresponding to a logical zero, after the reset time the driver was capable of pushing the charge in the correct direction

Figure 6.16: $VACT_1$: 3D ball and stick model of the wire's charge configuration, from this plot it is clear the metastability condition over the central couple which is expected for an even number of propagating couples and instead is occurring for an odd number of the same. Moreover, the second phase propagates the charge on the second molecule in the opposite state with respect to the expected one.

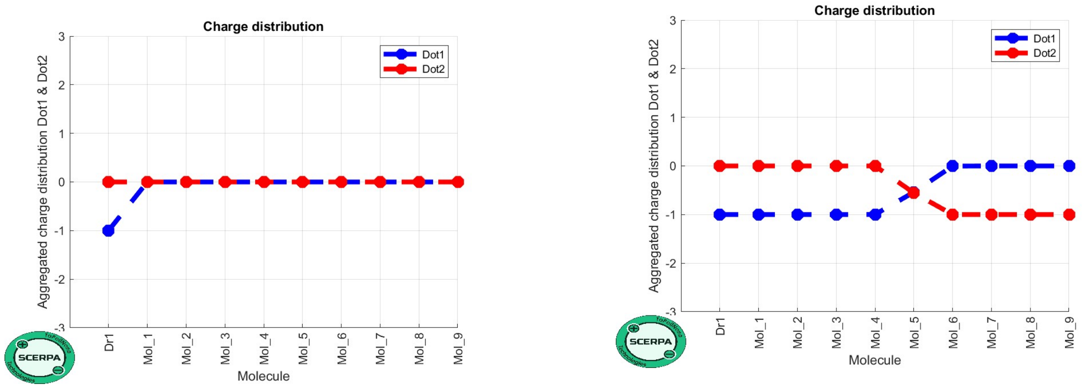

(a) First phase of the driver input corresponding to a reset state

(b) Second phase of the driver which after the reset is pushing an input state corresponding to a logical 1

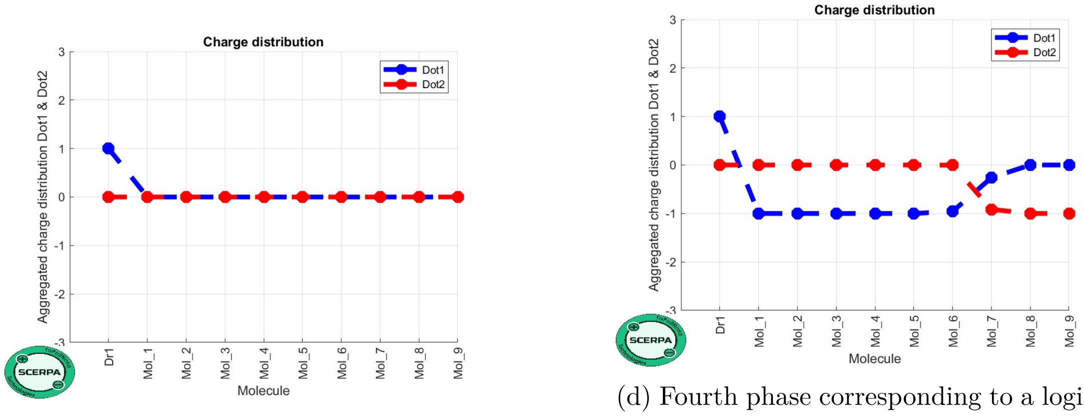

(c) Third phase used as reset to let the circuit be able to adjust itself and follow the second input

(d) Fourth phase corresponding to a logical 0, the driver was incapable of pushing the charge in the correct direction for the totality of the circuit, the wire stop propagates at the seventh molecule.

Figure 6.17: $VACT_1$: The 1 signal at the left of the wire did not correctly propagate. This highlights the need to define two drivers, one capable of pushing the charge from the left to the right of the wire and one doing the opposite.

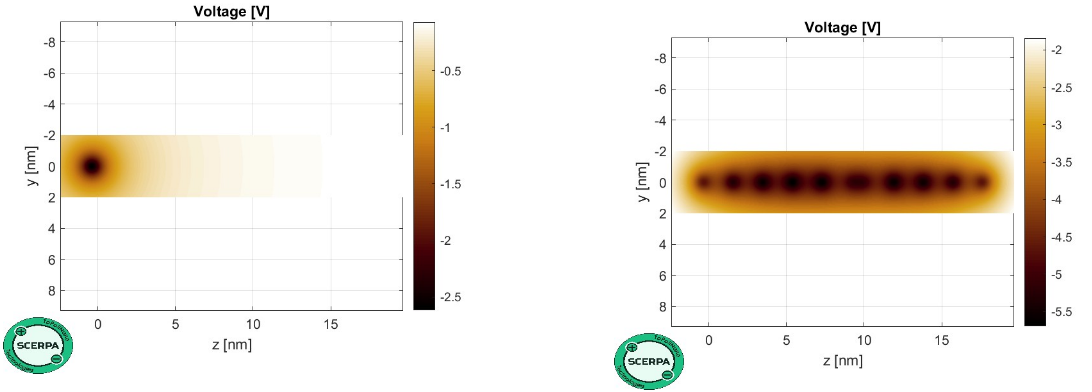

(a) Electrical potential of the first phase of the driver input corresponding to a reset state

(b) Second phase corresponding to the 1 signal

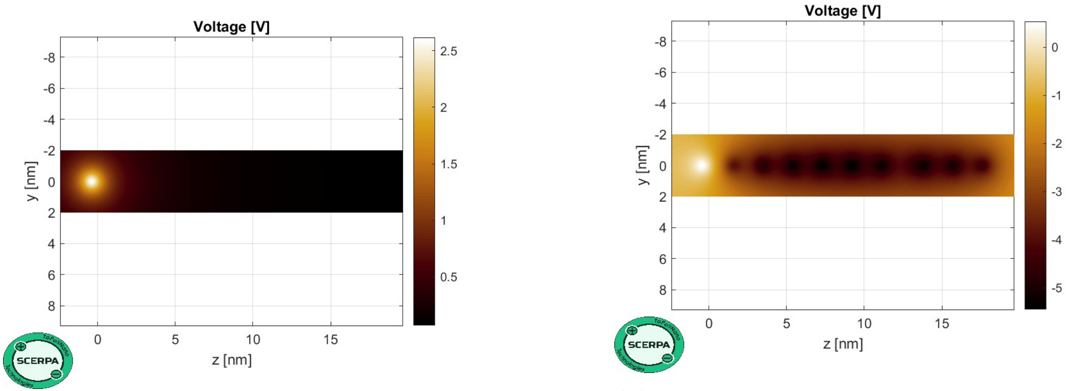

(c) Third phase used as reset to let the circuit be able to adjust itself and follow the second input

(d) Fourth phase corresponding to a logical 0, after the reset time the driver was capable of pushing the charge in the correct direction

Figure 6.18: $VACT_1$: The electrical potential is indicative of the charge state given as a result of the VACT used as a model for the molecules and the circuit's layout simulating a virtual tip placed at 5.5Åfrom the surface.

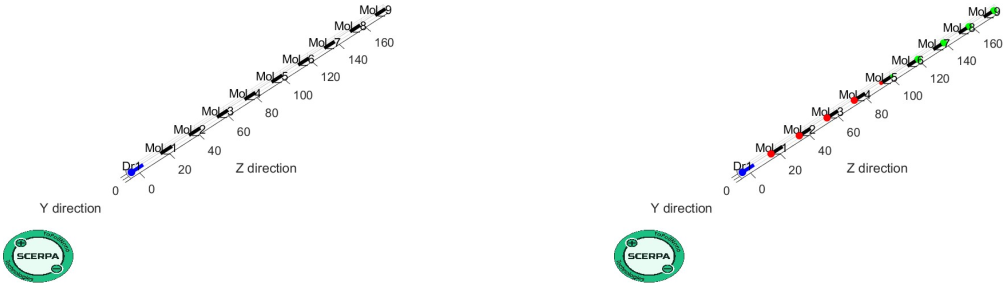

(a) First phase of the driver input corresponding to a reset state

(b) Second phase of the input driver which after the reset is pushing a 1 across the wire

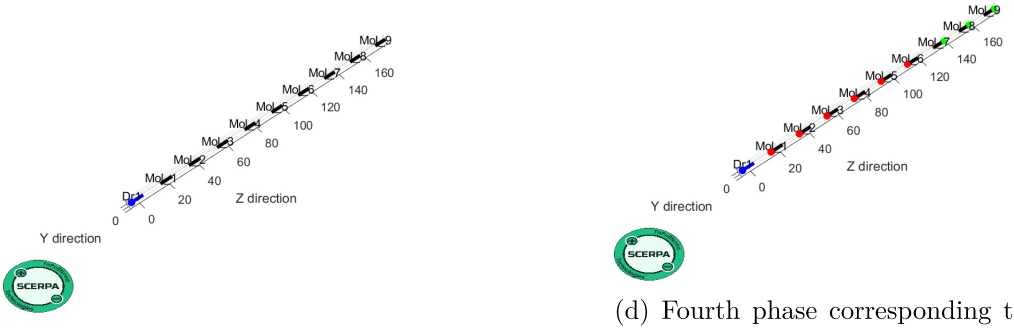

(c) Third phase used as reset to let the circuit be able to adjust itself and follow the second input

(d) Fourth phase corresponding to a logical zero, after the reset time the driver was capable of pushing the charge in the correct direction but the inversion occurs one molecule later to where it is expected.

Figure 6.19: $VACT_1$: 3D ball-stick model of the 1 signal propagating from the left to the right of the circuit. Despite the charge being pushed in the correct direction the signal is not able to reach the end of the wire thus an inversion occurs at the middle point of the circuit where a metastability condition is found.

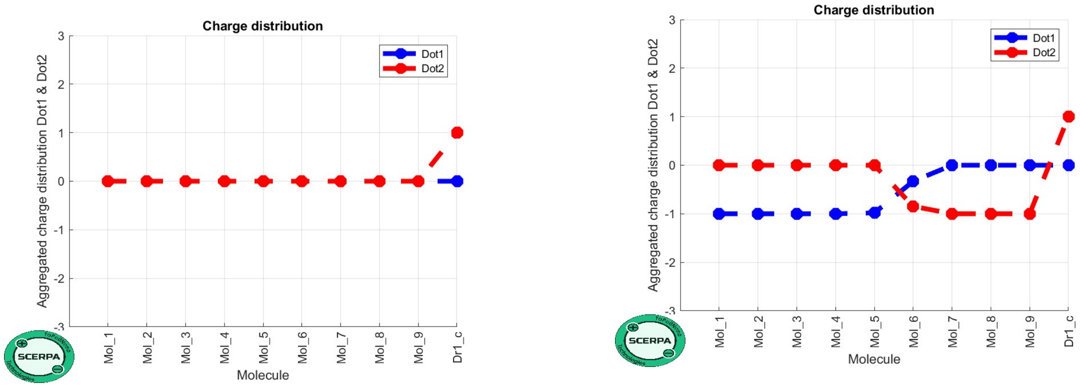

(a) First phase of the driver input corresponding to a reset state

(b) Second phase of the driver which after the reset is pushing an input state corresponding to a logical 1

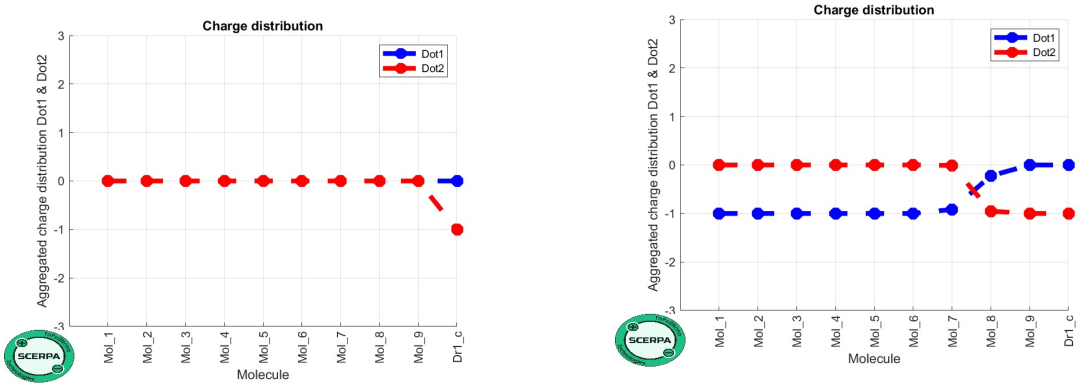

(c) Third phase used as reset to let the circuit be able to adjust itself and follow the second input

(d) Fourth phase corresponding to a logical 0, after the reset time the driver did not control the charge until the end of the circuit

Figure 6.20: $VACT_2$: 1D aggregated charges over the SiDB couples, the metastability over the second molecule is not expected and should not be present due to the fact that the number of couples is not even, thus the expected aggregated charge in the middle couple is the dot_1 occupied and the dot_2 unoccupied.

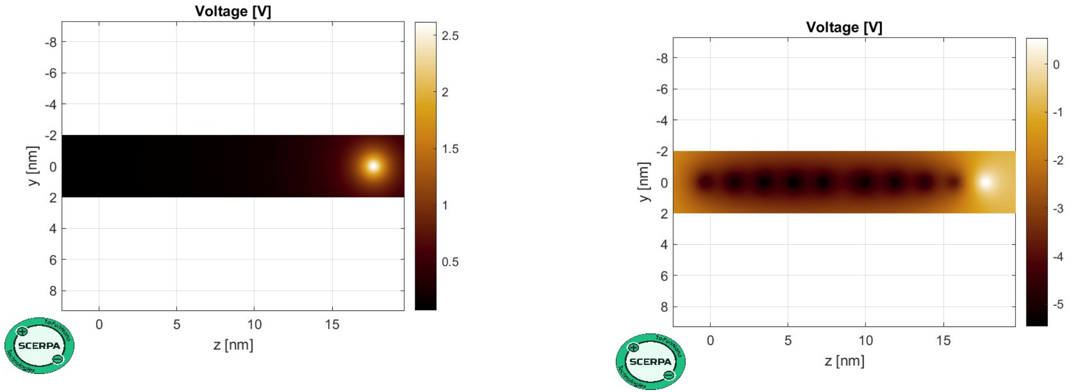

(a) Electrical potential of the first phase of the driver input corresponding to a reset state

(b) Second phase corresponding to the 1 signal

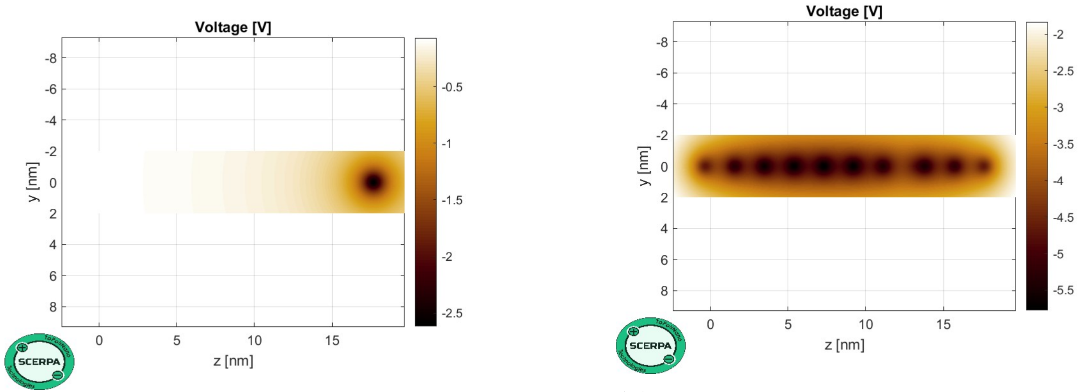

(c) Third phase used as reset to let the circuit be able to adjust itself and follow the second input

(d) Fourth phase corresponding to a logical 0, after the reset time the driver was capable of pushing the charge in the correct direction

Figure 6.21: $VACT_2$: The electrical potential is indicative of the charge state given as a result of the VACT used as a model for the molecules and the circuit's layout simulating a virtual tip placed at 5.5Åfrom the surface.

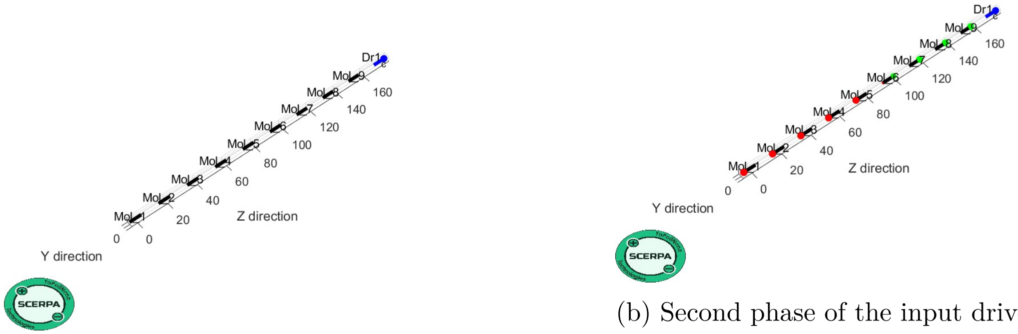

(a) First phase of the driver input corresponding to a reset state

(b) Second phase of the input driver which after the reset is pushing a 1 across the wire, it can be seen that the direction in which the charge is pushed is the opposite with respect to the driver's charge configuration.

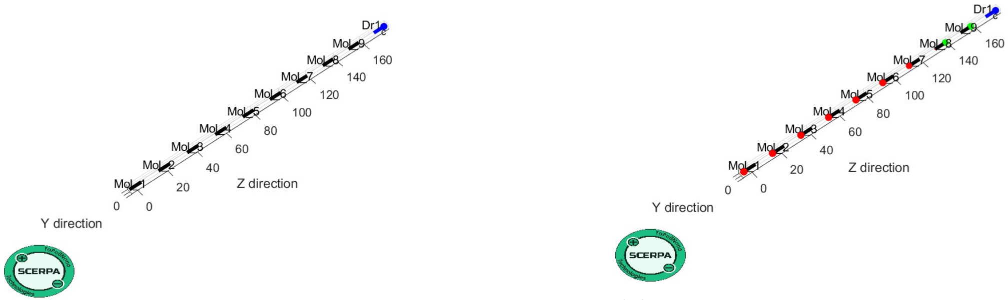

(c) Third phase used as reset to let the circuit be able to adjust itself and follow the second input

(d) Fourth phase corresponding to a logical zero, after the reset time the driver was capable of pushing the charge in the correct direction

Figure 6.22: $VACT_2$: 3D ball and stick model of the wire's charge configuration, from this plot it is clear the metastability condition over the central couple which is expected for an even number of propagating couples and instead is occurring for an odd number of the same. Moreover, the second phase propagates the charge on the second molecule in the opposite state with respect to the expected one.

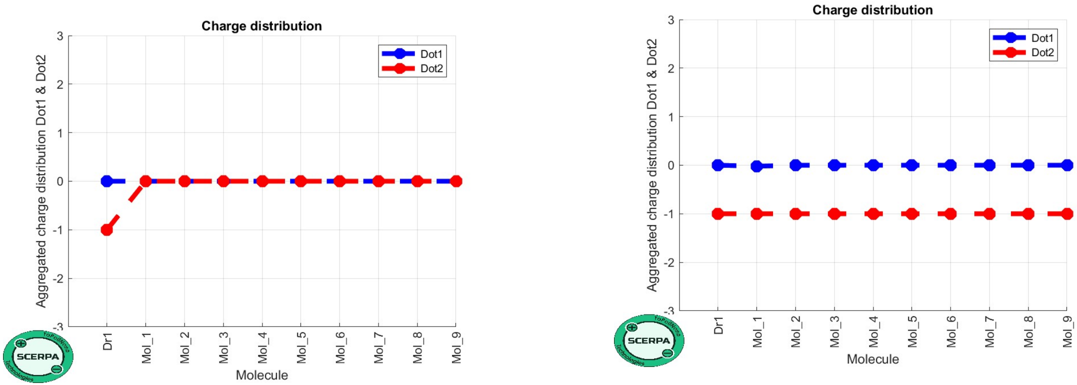

(a) First phase of the driver input corresponding to a reset state

(b) Second phase of the driver which after the reset is pushing an input state corresponding to a logical 1

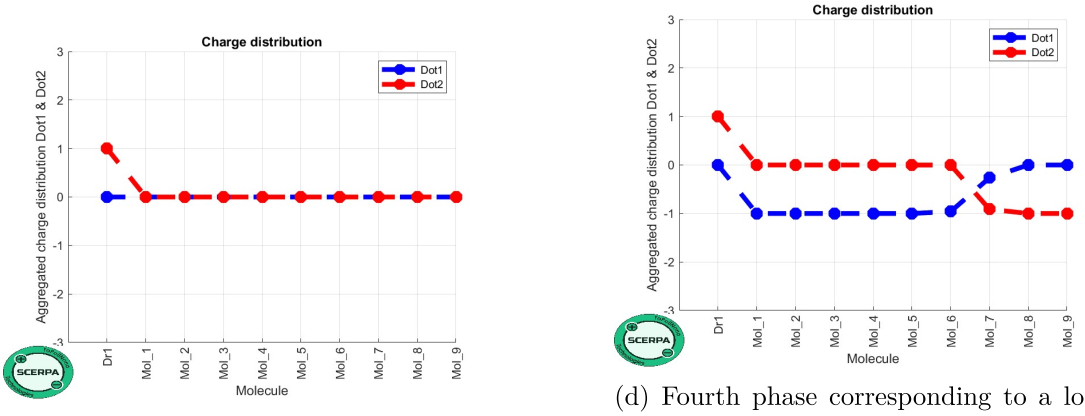

(c) Third phase used as reset to let the circuit be able to adjust itself and follow the second input

(d) Fourth phase corresponding to a logical 0, the driver was incapable of pushing the charge in the correct direction for all the couple, the wire stop propagates at the seventh molecule.

Figure 6.23: $VACT_2$: The 1 signal at the left of the wire did not correctly propagate. This highlights the need to define two drivers, one capable of pushing the charge from the left to the right of the wire and one doing the opposite.

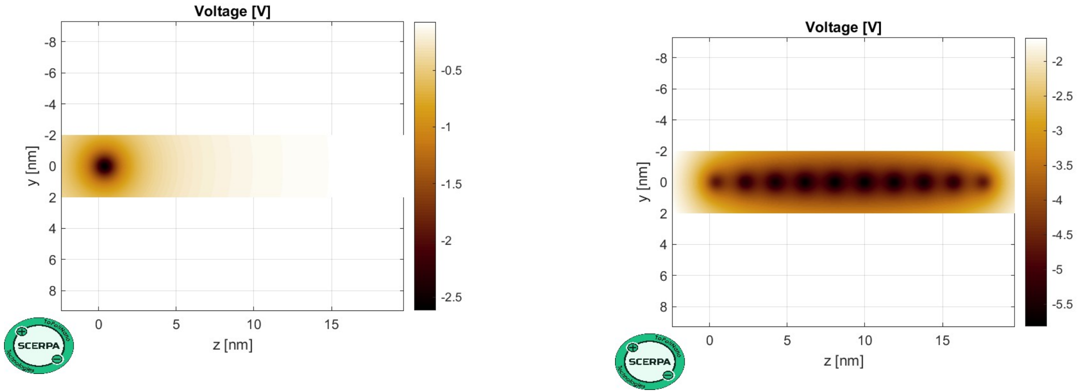

(a) Electrical potential of the first phase of the driver input corresponding to a reset state

(b) Second phase corresponding to the 1 signal

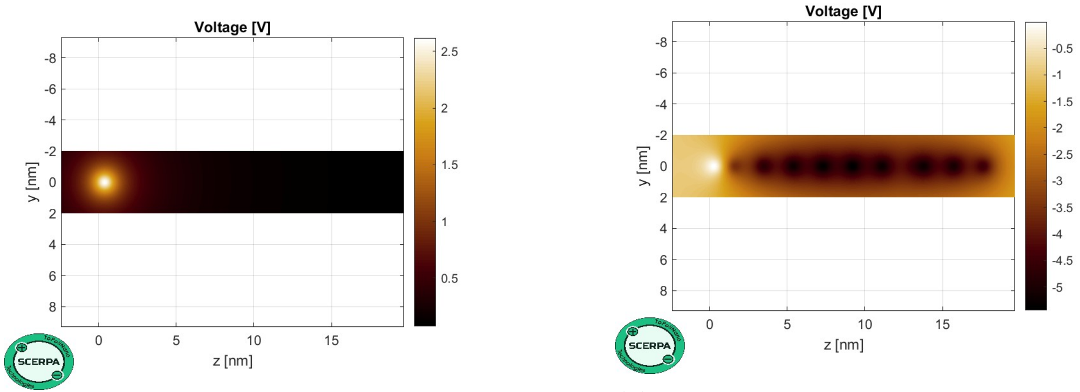

(c) Third phase used as reset to let the circuit be able to adjust itself and follow the second input

(d) Fourth phase corresponding to a logical 0, after the reset time the driver was capable of pushing the charge in the correct direction

Figure 6.24: $VACT_2$: The electrical potential is indicative of the charge state given as a result of the VACT used as a model for the molecules and the circuit's layout simulating a virtual tip placed at 5.5Åfrom the surface.

(a) First phase of the driver input corresponding to a reset state

(b) Second phase of the input driver which after the reset is pushing a 1 across the wire

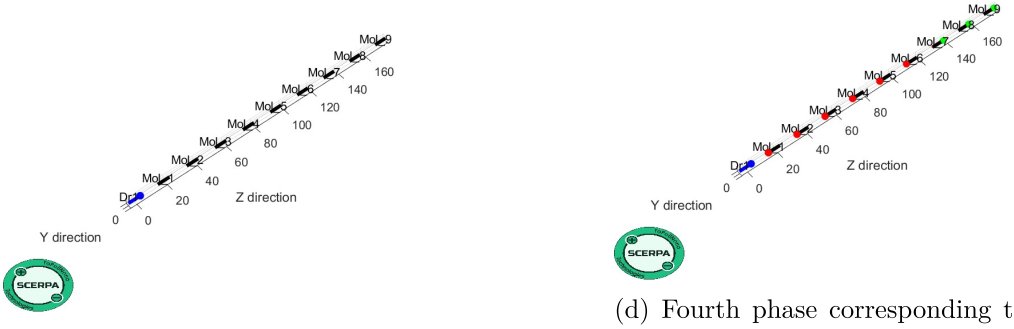

(c) Third phase used as reset to let the circuit be able to adjust itself and follow the second input

(d) Fourth phase corresponding to a logical zero, after the reset time the driver was capable of pushing the charge in the correct direction but the inversion occurs one molecule later to where it is expected.

Figure 6.25: $VACT_2$: 3D ball-stick model of the 1 signal propagating from the left to the right of the circuit. We can notice a specular behavior with respect to the previously implemented VACT, the charge for the fourth phase of the 1 signal isn't forcing the first molecule of the wire to assume the correct configuration.

From the potential figures 6.15, 6.18, 6.21, 6.24 the response of the circuit to the positive and negative charges in input can be seen and compared with the 1D charge configurations in 6.14, 6.17, 6.20, 6.23 and the 3D charge models in 6.16, 6.19, 6.22, 6.25. When looking at the 3D figures it should be paid attention to the fact that the molecule is pushing either a 0 or a 1 depending on the reduced/oxidized component so the charge on the successive molecule is either a 0 or 1 depending not on the position of the charge but on the state at which the driver is during the selected phase.

The results of these simulations highlighted the need to exploit two different drivers for simulating the correct charge pushing along the wire in both directions and thus define a distinguishable logic. The bistability condition highlights that the electrostatic of the wire is influencing the propagation of the charge, thus adapting the definition of the driver it is possible to eliminate it to the detriment of the information propagation along the wire. This consideration led to the implementation of a different VACT, not including the interaction among the two components of the basic SiDB couple, this was considered in the optics that the self-consistent algorithm could be capable of predicting the interaction among the molecules even if fed with a symmetric transcharacteristic not considering the couple interaction but fed with two symmetrical potentials.

6.3 Re-modeling of the BDL wire

The re-modeling of the wire passed through the definition of two symmetric external potentials ranging from -250 meV to +250 meV that has been considered to be independently fed to each DB, the band bending acting on each element has been calculated as:

$$V_{bb} = -(V_{ext} + \mu) \quad \text{with} \quad \mu = -0.231eV \tag{6.11}$$

where μ_- was the chemical potential chosen to obtain the optimal operational range for such a system as mentioned in [6]. Then the probabilities of carrier's transitions were calculated with the Fermi statistics, which parameters were also chosen following the directions in [6]:

$$\mathcal{P}^{DB_i}_{0\to-1}(V_{bb}) = \frac{1}{1 + e^{\frac{V_{bb}}{k_B T}}} \tag{6.12}$$

To be consistent in defining a couple of DBs propagating one electron only the negative transition probabilities were considered because the two dots were considered non-interacting thus the potential contribution for negative and positive charge transition is symmetric and equal as highlighted in 6.26 and 6.27, including positive transitions would have led to a neutral molecule definition which is still physically acceptable but not of interest for the treatment. The obtained reduced VACT is depicted in 6.28

For maintaining consistency in characterizing the DB pair hosting a single electron, only negative transition probabilities were accounted for. This choice has been made due to the assumption that the two dots are non-interacting, resulting in a symmetric and equivalent potential contribution for both negative and positive charge transitions. Incorporating positive transitions would have yielded a neutral molecule VACT which although physically acceptable, deviates from the specific focus of this analysis.

$$Q^{DB_i}_{Tot} = \mathcal{P}^{DB_i}_{0\to-1} \tag{6.13}$$

As a consequence of the redefinition of the potential available for the system, the drivers' VACTs have been redefined to keep a model representing a single dot in the defined potential range and to get the correct push for the charge to rearrange along the wire, the drivers' VACT are depicted in 6.29a and 6.29b. The simulation outcomes exclude the reset phase to avoid unnecessary verbiage and to get a full overview of how the wire is supposed to propagate the various inputs received from both directions, thus defining an exploitable binary logic.

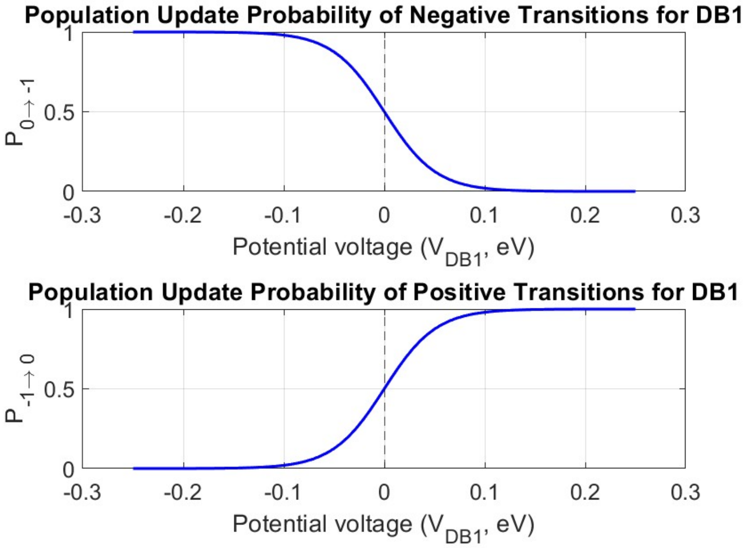

Figure 6.26: Positive and negative transition probabilities for the DB_1, it can be seen that they are symmetric as are obtained without interaction with the other component of the couple.

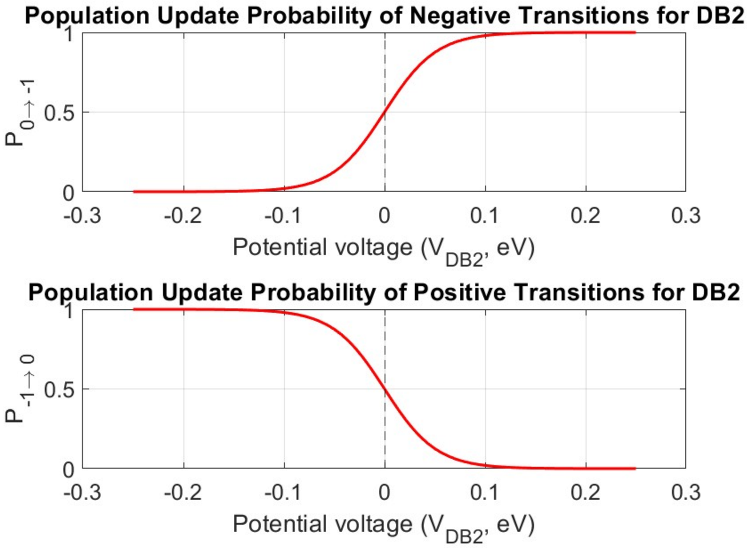

Figure 6.27: Positive and negative transition probabilities for the DB_2.

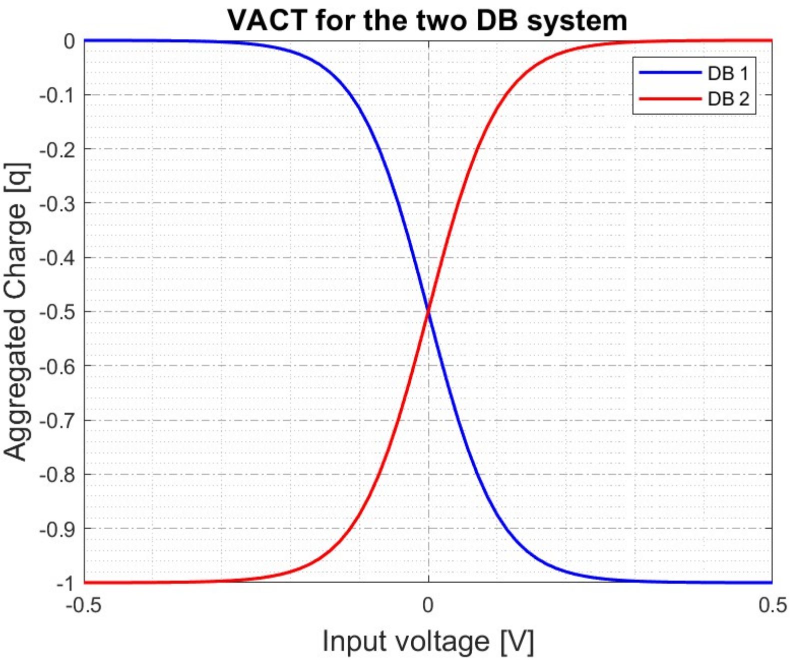

Figure 6.28: Symmetric VACT obtained from a simple Fermi statistic of two non-interacting DBs fed with symmetric potentials, to not alter the results when inverting the probability to get a reduced transcharacteristic the same have been flipped.

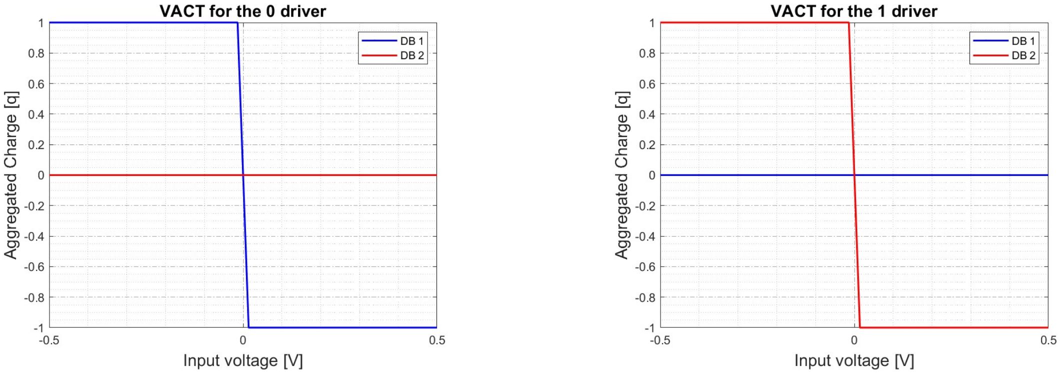

(a) VACT of the driver used as logical 0 on the right of the wire

(b) VACT of the driver used as logical 1 on the left of the wire

Figure 6.29: VACTs representing a perturber through a molecule having an oxidized characteristic for negative input voltage and reduced characteristic for positive input voltage. Using such a perturber the system correctly simulates a single atom acting as a perturber over the system, with this representation the driver has two possible charge states as the real perturber exploited to push the correct charge through the wire.

6.3.1 Results for the wire with non-interacting couples

The results for the non-interacting couple having an intermolecular distance of 5*3.84Åshowed that the intended information propagation is occurring properly, from the potential figures it is highlighted that both the positive drivers (0 propagating signals) that are the bright dot in 6.31a and 6.31c are capable of driving the wire in the correct configuration, the same occurs for the negative drivers (propagating the complementary 1) in 6.31b and 6.31d. From the 1D and 3D charge configuration 6.30 and 6.32 it can be appreciated the charge disposition along the wire follows the theoretical expectation derived from [13][1][4], this highlighted the algorithm's ability to simulate the molecular interaction between the wire's component starting from a non-interacting transcharacteristic. So as not to be too verbose the following are presented only the second and fourth phases of the signal, excluding the reset phases.

6.4 SCERPA simulation of the Y-OR

The simulation of the compact Y-Or presented in [6] was the next step to confirm if the self-consistent field algorithm was capable of simulating SiDB interactions across more than one dimension and if the implemented molecules are suitable for representing SiDB couples. The Y-shaped OR in the SCERPA's reference system was quite a challenge to correctly represent with the right distances. This was due to the rotations and the negative coordinates of the first atom of the molecules and the fixed step for both z and y directions was making the bi-dimensional spacing quite harsh the placing of the molecules with different spacing. The results are obtained as usual for two phases to get both 0/1 input signals, just like in the real-life circuit in the simulations an output perturber was used to fix the charge of the components at the output and pull the correct charge, thus the choice of the driver type was crucial to get the desired input push and output pull along the circuit. Due to the impossibility of defining a single atom molecule in SCERPA (even the driver earlier defined is composed of two atoms in which one always has a 0 net aggregated charge), the output perturber needed was added as an extra component concerning the Y-OR in [6]. However, the aggregated charge in the simulation results was found in good agreement with the results presented in previous papers [6] [4] and correctly simulated the OR gate.

In this discussion, the reset phase was not excluded to clarify a point around the driver choice: the 3D charge representation in the driver is not an accurate reflection of the charge state since it does not distinguish between positive and negative charges, for example, a driver can host the charge in the dot placed furthest with respect the first molecule of the circuit but still push a 1 across it like in 6.34d. For a clearer understanding of the charge in the circuit, it is recommended to consider the electric potential 6.33d and 6.35d which clearly highlights how the positive and negative drivers interact with the rest of the circuit but still the 3D charge images in 6.34 and 6.36 give a clear representation of the charge configuration along the gate.

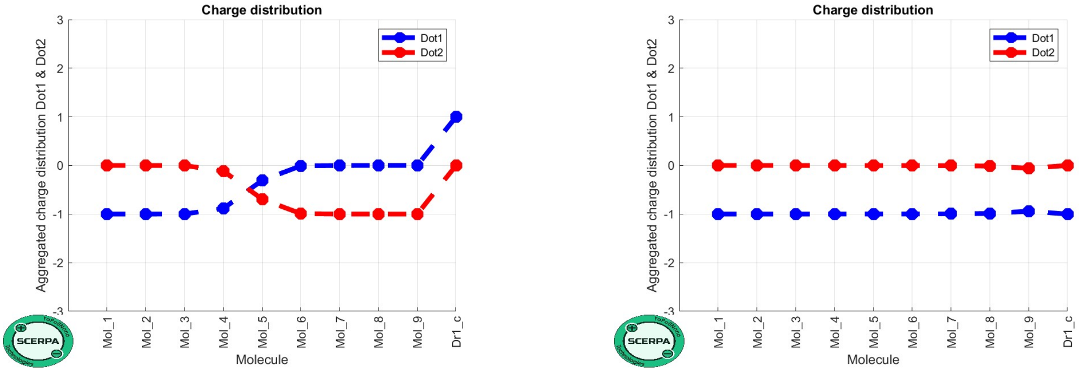

(a) 1D aggregated charge along the wire for the driver's second phase corresponding to a right propagating 1 signal.

(b) 1D aggregated charge along the wire for the driver's second phase corresponding to a right propagating 0 signal.

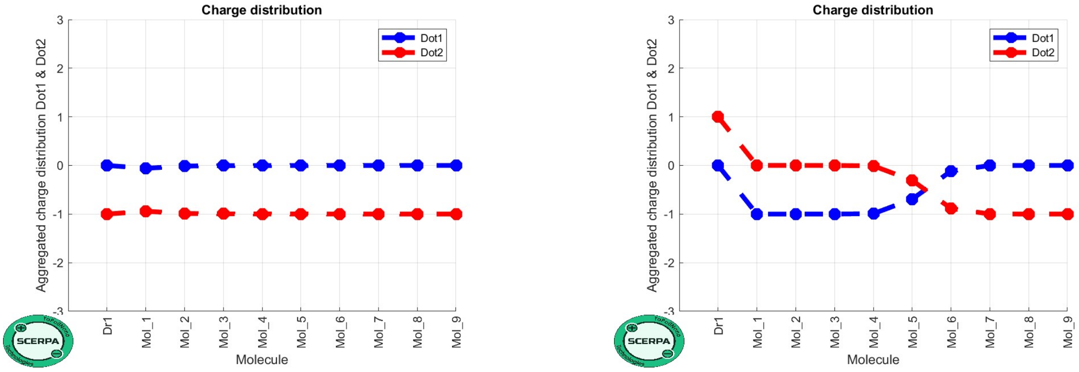

(c) 1D aggregated charge along the wire for the driver's second phase corresponding to a left propagating 1 signal.

(d) 1D aggregated charge along the wire for the driver's second phase corresponding to a left propagating 0 signal.

Figure 6.30: 1D aggregated charge of the wire with 0 input signal fed to the right and 1 input signal fed to the left of the circuit with the intermolecular distance set as $5 \cdot 3.84$Å, as the wire demonstrated in previous researches [5][6][4][7] was able to define a binary logic.

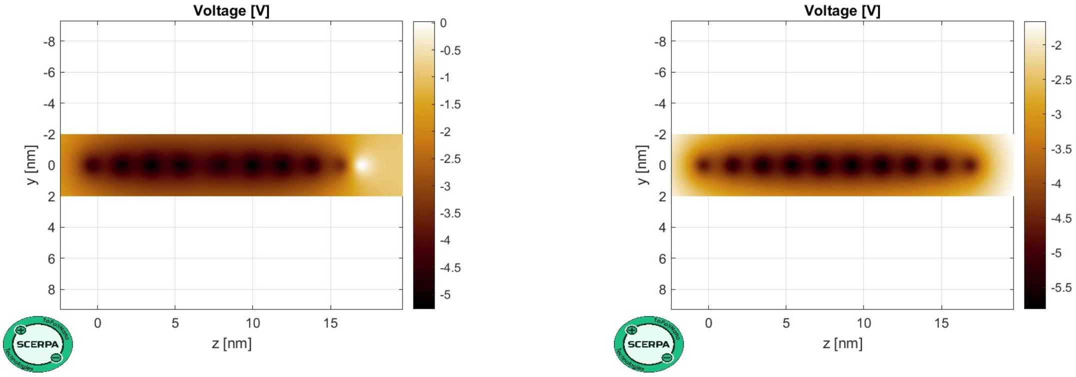

(a) Electrostatic potential along the wire for the driver's second phase corresponding to a right propagating 1 signal.

(b) Electrostatic potential along the wire for the driver's second phase corresponding to a right propagating 0 signal.

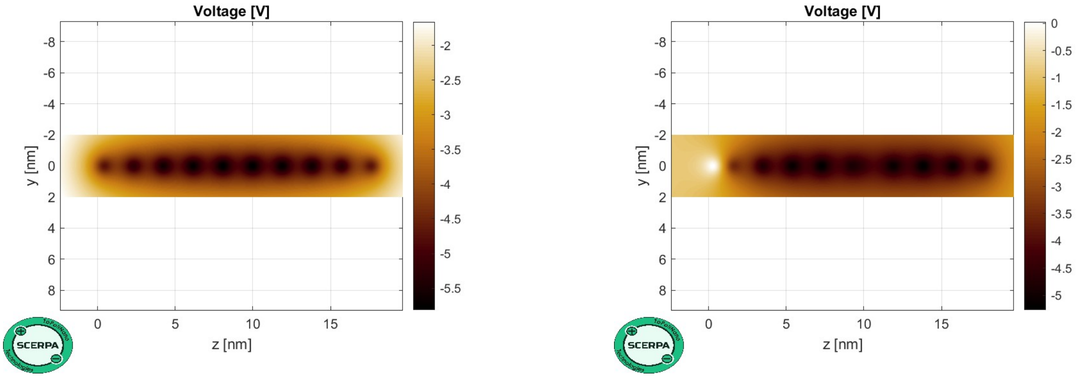

(c) Electrostatic potential along the wire for the driver's second phase corresponding to a left propagating 1 signal.

(d) Electrostatic potential along the wire for the driver's second phase corresponding to a left propagating 0 signal.

Figure 6.31: Electrostatic potential of the wire with 0 input signal fed to the right and 1 input signal fed to the left of the circuit with the intermolecular distance set as $5 \cdot 3.84$Å.

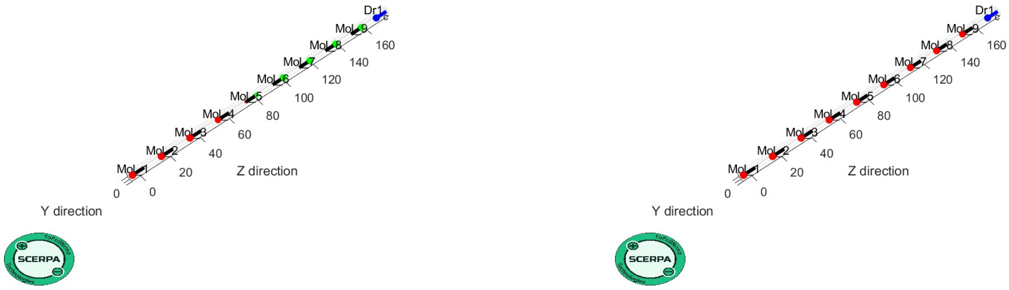

(a) 3D ball and stick model of the aggregated charge along the wire for the driver's second phase corresponding to a right propagating 1 signal.

(b) 3D ball and stick model of the aggregated charge along the wire for the driver's second phase corresponding to a right propagating 0 signal.

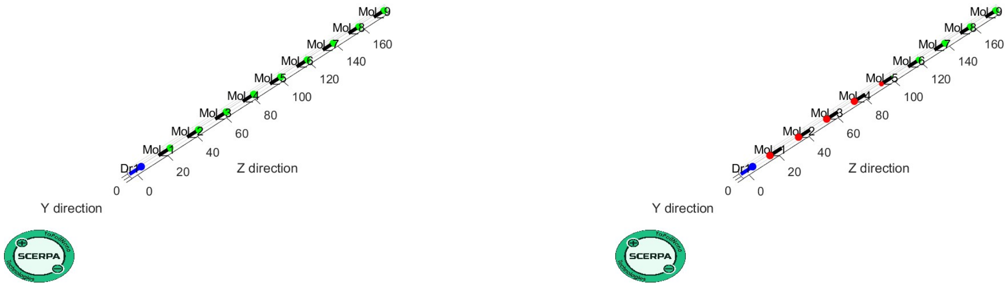

(c) 3D ball and stick model of the aggregated charge along the wire for the driver's second phase corresponding to a left propagating 1 signal.

(d) 3D ball and stick model of the aggregated charge along the wire for the driver's second phase corresponding to a left propagating 0 signal.

Figure 6.32: 3D ball and stick model of the aggregated charge along the wire's molecules with 0 input signal fed to the right and 1 input signal fed to the left of the circuit and intermolecular distance set as $5 \cdot 3.84$Å.

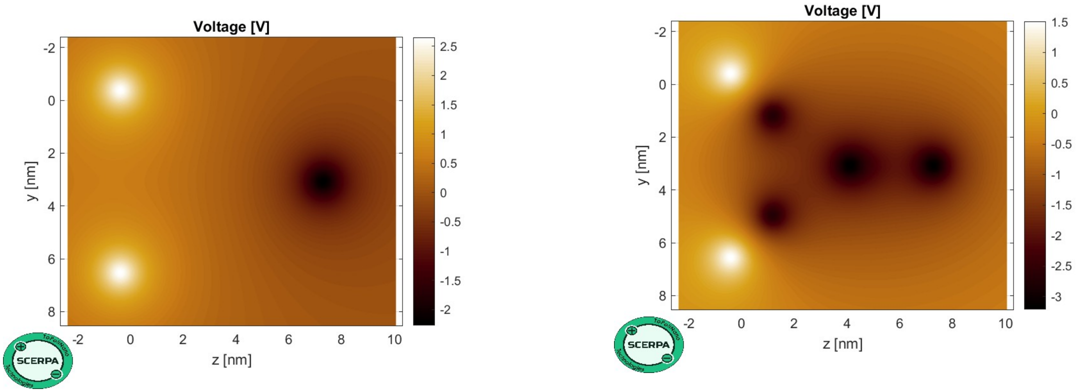

(a) Electrostatic potential of the Y-OR in the first reset phase.

(b) Electrostatic potential for the circuit corresponding to a 0 input signal on both the arms of the Y.

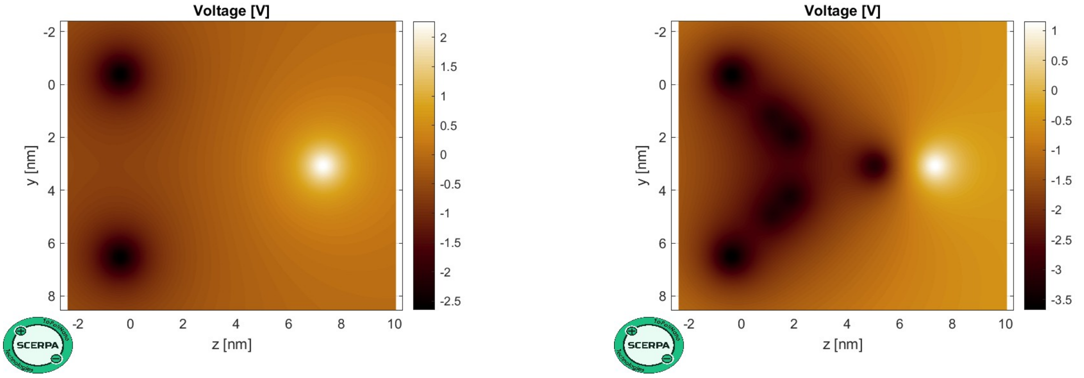

(c) Electrostatic potential of the Y-OR in the third phase that corresponds to a reset and change of input.

(d) Electrostatic potential for the circuit corresponding to a 1 input signal on both the arms of the Y.

Figure 6.33: Electrostatic potential for the Y-OR, the bright protrusions represent a driver with an excess of holes, useful to represent the absence of signal for a system propagating electrons like the DBs with reduced VACT defined in this work.

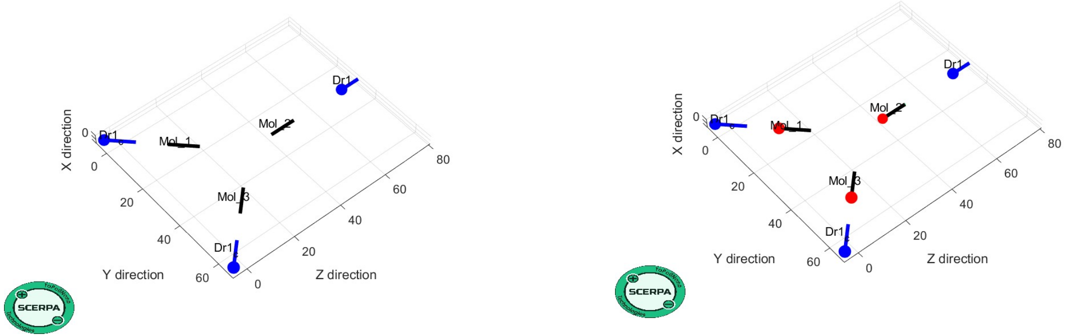

(a) 3D charge model of the Y-OR in the first reset phase.

(b) 3D charge model of the Y-OR for the circuit corresponding to a 0 input signal on both the arms of the Y.

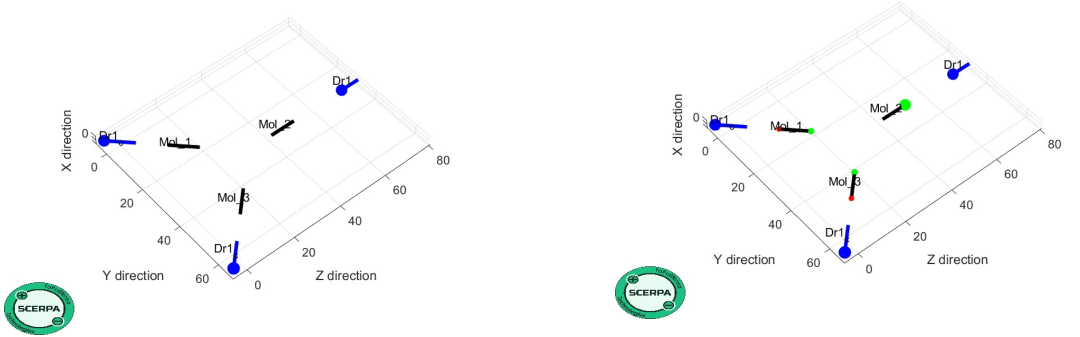

(c) 3D charge model of the Y-OR in the third phase that corresponds to a reset and change of input.

(d) 3D charge of the circuit corresponding to a 1 input signal on both the arms of the Y, as expected we can appreciate the bistability condition in both arms.

Figure 6.34: With the 3D charge figure we can clearly appreciate the aggregated charge along the circuit which matches the one obtained in the experimental studies of [6] .

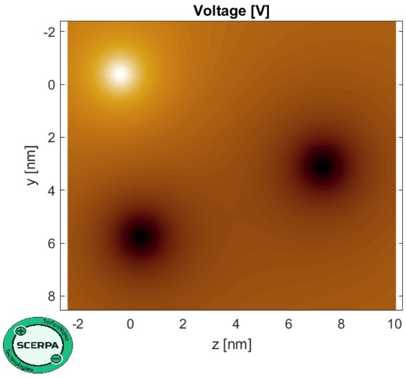

(a) Electrostatic potential of the Y-OR in the first reset phase.

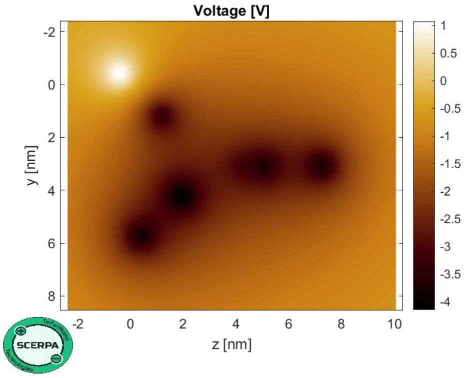

(b) Electrostatic potential for the circuit corresponding to a 1 input signal on the bottom arm and 0 input signal on the topmost arm.

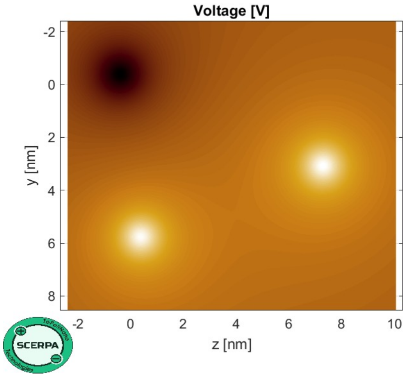

(c) Electrostatic potential of the Y-OR in the third phase that corresponds to a reset and change of input.

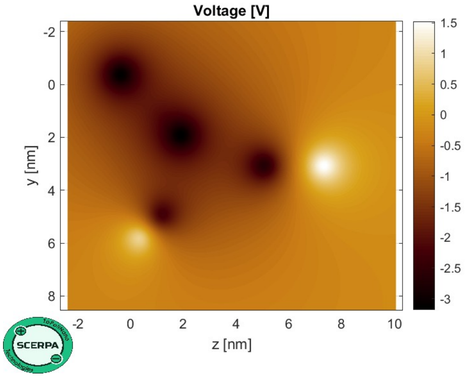

(d) Electrostatic potential for the circuit corresponding to a 0 input signal on the bottom arm and 1 input signal on the topmost arm.

Figure 6.35: Electrostatic potential for the Y-OR, the bright protrusions represent a driver with an excess of holes, useful to represent the absence of signal for a system propagating electrons like the DBs with reduced VACT defined in this work.

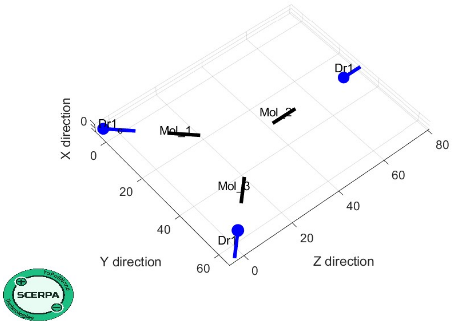

(a) 3D charge model of the Y-OR in the first reset phase.

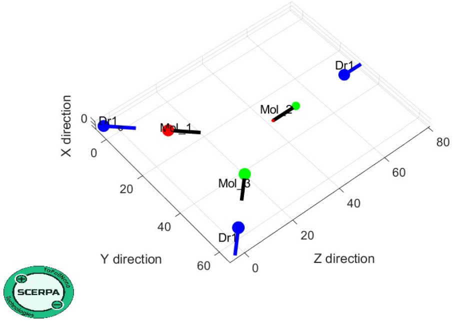

(b) 3D charge model of the Y-OR for the circuit corresponding to a 1 input signal on the bottom arm and 0 input signal on the topmost arm.

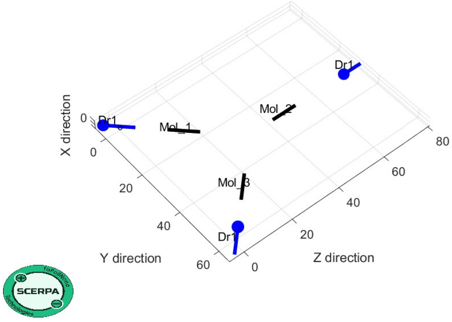

(c) 3D charge model of the Y-OR in the third phase that corresponds to a reset and change of input.

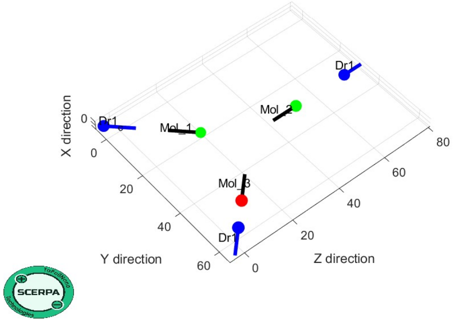

(d) 3D charge model of the Y-OR for the circuit corresponding to a 0 input signal on the bottom arm and 1 input signal on the topmost arm.

Figure 6.36: With the 3D charge figure it is possible to appreciate the aggregated charge along the circuit which matches the one obtained in the experimental studies of [6] also for the 10 and 01 input signals, with these images it is clear that this FOM is not indicative of the actual charge state of the driver.

Part III

Post-Processing

Chapter 7

Circuit analysis

Beyond the 1D aggregated charge, electrostatic potential, and 3D charge model, SCERPA's simulations have a Matlab .mat output file that includes all the circuit settings, inputs, and outputs. From these files, it is possible to calculate all the quantities of interest for the FCN circuit, for example, from the potential it is possible to derive the electric field and the charge density thus enabling a full understanding of the electrostatic of the circuit under analysis. In the following, some of these figures of merit are introduced to give an idea of the possible analysis that can be derived from these simulations. In particular, the electric field along the two directions has been calculated with the Matlab function gradient and then validated with a differential approach starting from the electrostatic potential:

$$E^z_{i,j} = \frac{V_{i+1,j} - V_{i-1,j}}{2} \tag{7.1}$$

$$E^y_{i,j} = \frac{V_{i,j+1} - V_{i,j-1}}{2} \tag{7.2}$$

where $V_{i,j}$ is the potential in the i-th position on the z axes and the j-th position on the y-axes calculated with the potential-evaluating algorithm included with SCERPA. Examining the electric field in the z and y directions helps in the understanding of the forces influencing charges in those directions. This perspective can hint at how molecules react to their input field, giving an understanding of the forces guiding the information across the circuit. After calculating the EF the charge density in every point of the space was retrieved as the divergence of the electric field multiplied by the vacuum permittivity. The charge density distribution reveals how the electric charge is spatially distributed across the circuit, highlighting how the charge transfer and carriers accumulate due to the electric field imposed by the user.

$$\frac{\rho}{\varepsilon_0} = \nabla \cdot \mathbf{E} \tag{7.3}$$

Moreover, the intensity of the electric field serves as a global indicator of the overall strength of the electric field identifying regions of varying field intensity it is possible to understand the strength of the interaction between molecules, it was straightforwardly calculated as:

$$I = \sqrt{E_z^2 + E_y^2} \tag{7.4}$$

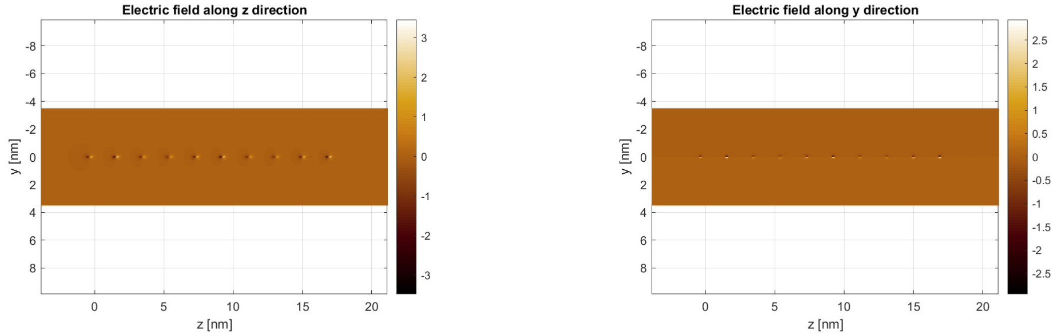

(a) Electric field along the z direction.

(b) Electric field along the y direction.

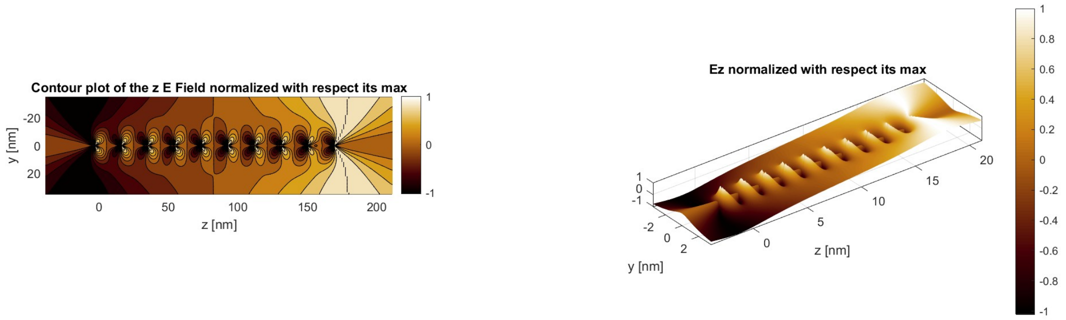

(c) Contour plot of the electric field along z, it can be used to evaluate the field stability.

(d) Normalized E_z.

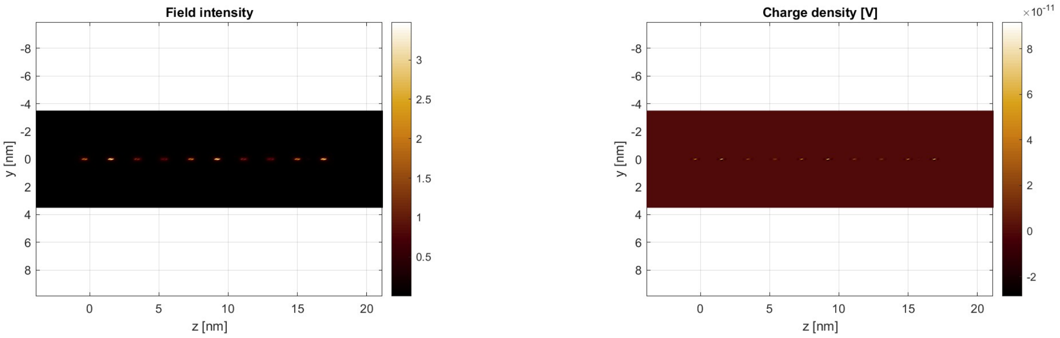

(a) Electric field intensity.

(b) Charge density.

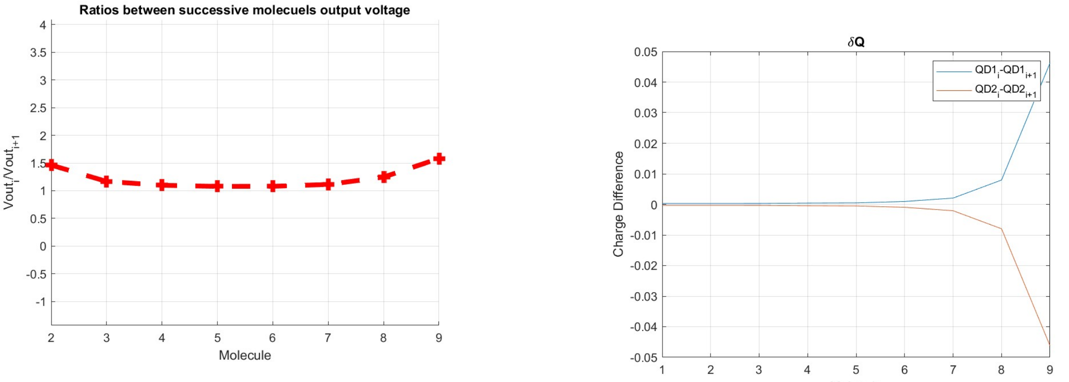

(c) Ratio of the output voltage of a molecule with respect to the successive, it can be an indicator of how much energy is lost on the information propagation on successive steps.

(d) Change in charge between dot_1 and dot_2 within consecutive molecules, can be an indicator of molecule's coupling.

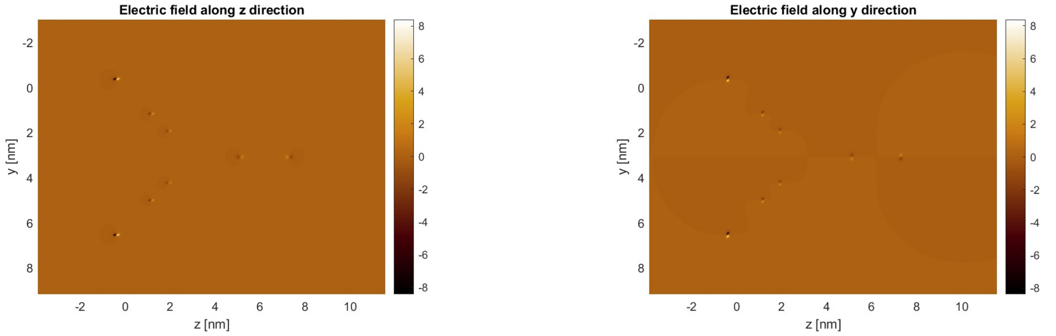

(a) Electric field along the z direction.

(b) Electric field along the y direction.

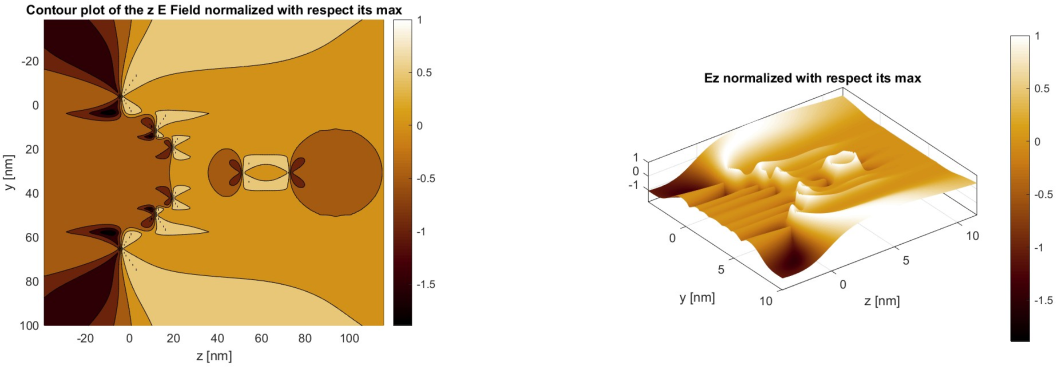

(c) Contour plot of the electric field along z, it can be used to evaluate the field stability.

(d) Normalized E_z.

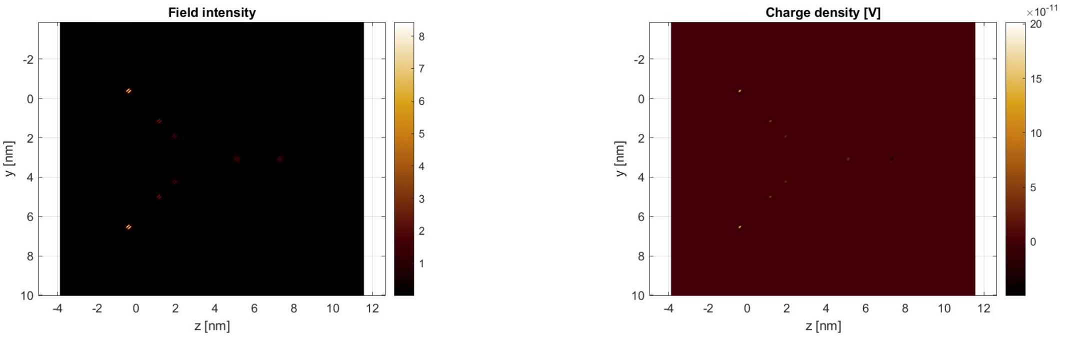

(a) Electric field intensity.

(b) Charge density.

Chapter 8

Conclusions

In conclusion, with this master's thesis, we highlighted the possibility of exploiting the MoSQuiTo methodology firstly deployed for molecular circuit and QCA technology to characterize the atomic silicon dangling bond framework, thus underlying the agility of the approach that could be virtually employed in the modeling of any FCN technology. Employing the SCERPA algorithm for atomic SiDBs, traditionally used in molecular circuits we proved the flexibility and effectiveness of the approach for investigating the dynamics of atomic circuits. The adaptability and reliability of the results confirm the MoSQuiTo methodology and the SCERPA algorithm as a solid set of tools for studying complex field-coupled circuits without the excessive computational effort due to ab initio calculations.

To validate the efficacy of the proposed approach a comparison with previous works was carried on, some of them completed with experimental evidence further confirming simulation results. The basic behavior of a SiDB couple was determined firstly with a simulated annealing algorithm and later by the simple electrostatic of the system thus relying on the self-consistency of the algorithm to model the interaction between components. The simulations were benchmarked against the behavior of a binary dotted logic wire and a Y-shaped OR gate. This comparative analysis provided a validation of the SCERPA algorithm in capturing the dynamics of atomic silicon dangling bond interactions.

The outcomes of this thesis contribute to the improvement of the knowledge in FCN, offering a valuable alternative perspective on the behavior of a novel technology such as silicon dangling bonds. The comparison with established logic wire and gate models adds depth to the validation process, emphasizing the algorithm's reliability and applicability in diverse scenarios.

In summary, this master's thesis not only explores the behavior of silicon dangling bonds in the context of field-coupled nanocomputing but also underscores the adaptability and reliability of the SCERPA algorithm. As we navigate the ever-evolving landscape of nanotechnology, these insights pave the way for future research, and innovative and more convenient approaches to explore the nanocomputing realm.

Bibliography

[1] R. A. Wolkow. Silicon atomic quantum dots enable beyond-cmos electronics. *Lecture Notes in Computer Science (including subseries Lecture Notes in Artificial Intelligence and Lecture Notes in Bioinformatics)*, eds Neal, G. and Anderson, S. B.(1):33–58, 2014.

[2] Y. Ardesi, A. Pulimeno, M. Graziano, F. Riente, and G. Piccinini. Effectiveness of molecules for quantum cellular automata as computing devices. *Journal of Low Power Electronics and Applications*, 8(24):1–19, 2018.

[3] V. Arima, M. Iurlo, L. Zoli, S. Kumar, M. Piacenza, F. Della Sala, F. Matino, G. Maruccio, R. Rinaldi, F. Paolucci, M. Marcaccio, P. G. Cozzi, and A. P. Bramanti. Toward quantum-dot cellular automata units: thiolated-carbazole linked bisferrocenes. *Nanoscale*, 4(4):813–823, 2011.

[4] T. R. Huff. Binary atomic silicon logic. *Nature Electronics*, 1(12):636–643, 2018.

[5] T. R. Huff. Atomic white-out: Enabling atomic circuitry through mechanically induced bonding of single hydrogen atoms to a silicon surface. *Nature Communications*, 11(9):8636–8642, 2017.

[6] S. S. H. Ng. Siqad: A design and simulation tool for atomic silicon quantum dot circuits. *IEEE Transactions on Nanotechnology*, 19(8):137–146, 2020.

[7] M. Taucer. Silicon dangling bonds: Non-equilibrium dynamics and applications. *University of Alberta*, 2015.

[8] G. Piccinini, Y. Ardesi, and M. Graziano. A model for the evaluation of monostable molecule signal energy in molecular field-coupled nanocomputing. *Journal of Low Power Electronics and Applications*, 12(1):1–22, 2022.

[9] Craig S. Lent and P. Douglas Tougaw. A device architecture for computing with quantum dots. *Proceedings of the IEEE*, 85(4):541–557, 1997.

[10] Yuri Ardesi, Giovanna Turvani, Mariagrazia Graziano, and Gianluca Piccinini. Scerpa simulation of clocked molecular field-coupling nanocomputing. *IEEE Transactions on Very Large Scale Integration (VLSI) Systems*, 29(3):558–567, 2021.

[11] P. Douglas Tougaw and Craig S. Lent. Dynamic behavior of quantum cellular automata. *Journal of Applied Physics*, 80(8):4722–4736, 1996.

[12] R. Achal. Lithography for robust and editable atomic-scale silicon devices and memories. *Nature Communications*, 9(1):2788, 2018.

[13] N. H. Chiu. Poissolver: a tool for modelling silicon dangling bond clocking networks. *IEEE 20th International Conference on Nanotechnology (IEEE-NANO)*, 29(7):1–6, 2020.

[14] Y. Ardesi, R. Wang, G. Turvani, G. Piccinini, and M. Graziano. Scerpa: A self-consistent algorithm for the evaluation of the information propagation in molecular field-coupled nanocomputing. *IEEE TRANSACTIONS ON COMPUTER-AIDED DESIGN OF INTEGRATED CIRCUITS AND SYSTEMS*, 39(10):12, 2020.

[15] S. S. H. Ng. Computer-aided design of atomic silicon quantum dots and computational applications. *The University of British Columbia*, 10.14288/1.0392909, 2020.

[16] Hsi Nien Chiu. Simulation and analysis of clocking and control for field-coupled quantum-dot nanostructures. *The University of British Columbia*, 2017.